Mechanical Properties, Durability, and Life-Cycle Analysis of Self-Consolidating Concrete Mixtures Made with Blended Portland Cements Containing Fly Ash and Limestone Powder

Kemal Celik [a] , Cagla Meral [a,b], A. Petek Gursel [a], P.K. Mehta [a], Arpad Horvath [a], Paulo J.M. Monteiro [a,*]

[a] Department of Civil and Environmental Engineering, University of California, 94720 Berkeley, CA, USA

[b] Department of Civil Engineering, Middle East Technical University, 06800 Ankara, TURKEY

*Corresponding author: Tel.: +1 (510) 643-8251; Fax: +1 (510) 643-8928; E-mail address: monteiro@ce.berkeley.edu; Department of Civil and Environmental Engineering, 725 Davis Hall, University of California, Berkeley, CA 94720-1710, USA

Abstract

This paper reports the composition and properties of highly flowable self-consolidating concrete (SCC) mixtures made of high proportions of cement replacement materials such as fly ash and pulverized limestone instead of high dosage of a plasticizing agent or viscosity-modifying chemical admixtures. Self-consolidating concrete mixtures

are being increasingly used for the construction of highly reinforced complex concrete elements and for massive concrete structures such as dams and thick foundation. In this study, by varying the proportion of portland cement, fly ash, and limestone powder, SCC mixtures with different strength values were produced, and the properties of both fresh and hardened concrete were determined. Sustainability criterion was assessed based on the life-cycle assessment (LCA) approach, which is particularly crucial for a methodical analysis and quantification of the overall environmental impacts of concrete production. This study quantifies the reduction in global warming potential based on a LCA of high-volume fly ash concrete.

Keywords: self-consolidating concrete (SCC); fly ash; life-cycle assessment (LCA); limestone powder; global warming potential (GWP); sustainability

1 Introduction

According to data compiled by the U.S. Geological Survey (USGS) in 2011 [1], the yearly global production of portland cement was about 3.4 billion metric tonnes (mt). Considering typical concrete mix proportions for ordinary concrete [2], this amount of cement is incorporated into approximately 28 billion mt of concrete, which requires 23 billion mt of aggregates and 2.3 billion mt of fresh water, leading to an annual global average consumption rate of about 4 mt of concrete per person. The massive production and consumption cycle of concrete has substantial environmental impact.

Carbon dioxide (CO_2) emissions associated with portland cement production is one of the major sustainability issues facing the concrete industry today. Although considerable gains in energy efficiency during cement production manufacturing have been realized over the last two decades, according to industry data [3], about 866 kg of CO_2 are being generated for every 1000 kg of clinker produced. Roughly 52% of these emissions come from the calcination of limestone, which is the main raw material for making portland-cement clinker. For every tonne of calcium carbonate calcined in the kiln to form calcium oxide, 440 kg of CO_2 are released into the atmosphere as the chemical reaction progresses. The combustion of fuel required to generate the heat necessary for the clinker minerals forming reactions to take place accounts for the remaining CO_2 emissions.

As a result, considering an average clinker factor (kg of clinker per kg of cement) of 0.78 [3], annual worldwide CO_2 emissions from cement production add up to almost 2.3 billion mt, which is nearly 7% of the global emissions from fossil-fuel [2]. For an average of 918 kg of CO_2 per tonne of cement [4], the U.S cement industry generated about 56 million mt of CO_2 based on the 2010 portland cement production rate, that is 61 million mt [1]. These numbers correspond to direct emissions only, i.e., those generated in the cement factory. Based on economic input-output lifecycle assessment (EIO-LCA) analysis using the U.S. data [5], life-cycle emissions associated with cement manufacturing are expected to be 13% higher than direct emissions.

While the current environmental impact of the concrete industry is indeed considerable, the increased use of supplementary cementitious materials (SCMs) offer a possible solution in reducing global CO_2 emissions. A recent study involving business leaders and academics [6] singled out construction materials as one of the seven most promising technologies for investment (together with wind, biofuels, photovoltaics, and concentrating solar power, nuclear, and building efficiency). The report concludes that within the construction materials sector, "the biggest single opportunity for CO_2 reduction is a low-carbon cement," and that annual savings of 1 billion mt of CO_2 could be reached through the concrete sector if 50% of portland cement were replaced by a low-carbon alternative.

In order to achieve such a level of CO_2 reductions, the industry must embrace a comprehensive, integrated approach that necessarily involves the use of less concrete for new structures, consumption of less cement in concrete mixtures, and use of less clinker for making cements [7].

Replacing half of portland cement would require about 1.7 billion mt of alternative materials, according to USGS data [1]. High-volume fly ash (HVFA) concrete has been used successfully for many years in numerous applications with technical and environmental advantages as compared to conventional portland cement concrete, and its use is expected to keep increasing over time [7-9]. Yet already the global availability of fly ash is roughly 800 million mt [10], which is about 47% of the overall amount of

materials needed. Thus, it is easy to conclude that other materials, such as limestone powder, must be increasingly brought into the mix.

Limestone powder (L) as calcite (or crystalline $CaCO_3$) is a widely available resource that has been added to cement and concrete in small volumes for many years, particularly in Europe. Recent research has shown that larger amounts can be successfully used in low water-cementitious materials ratio (w/cm) systems to conserve portland cement [11, 12]. The added limestone has two main functions. It acts as a limited participant in the hydration process at early ages and/or as a relatively inert calcareous filler depending on levels of calcite and replacement ratio [13, 14]. As the portland cement hydrates, the ground $CaCO_3$ reacts with various calciumaluminate hydrates to form high and low forms of carboaluminates [15]. Calcium hemicarboaluminate forms an early hydration product in calcite containing ordinary portland cement (OPC) blends. After about 28 days, it converts nearly completely to calcium monocarboaluminate, a stable AFm phase [15]. Thermodynamic calculations and experimental observations showed that monocarboaluminate formation is favored instead of monosulfoaluminate [16]. The available sulfate reacts with water and calcium hydroxide, crystalizing as ettringite [16, 17]. Due to additional ettringite formation, the total volume of the hydrated phase increases, and the overall porosity decreases [17].

This paper presents a study on the development of low-cost, environmental-friendly, self-consolidating concrete mixtures with high-volume fly ash (HVFA) and limestone powder (L).

Self-consolidating concrete (SCC) has been increasingly used in the field due to several advantages when compared to conventional concrete, including shortened placement time, labor savings, improved compaction, and better encapsulation of rebar. However, typical SCC mixes usually have an excessively high cement content, high heat of hydration, and utilize a high dosage of high-performance superplasticizers and viscosity-modifying agents [18-22]. Developed herein are self-consolidating concrete mixtures with low cement content (less than 250 kg/m^3), and a limited amount of a low range superplasticizer, and without any viscosity modifying agent, with ternary blends of cementing material containing portland cement, limestone powder and fly-ash. The mechanical properties and durability performance of these "greener concrete mixes" are presented. The properties determined of the fresh concrete include the slump flow, normal consistency, and setting time. Those of the hardened concrete investigated include the compressive strength, chloride-ion penetration, water absorption, and gas permeability.

In addition, the environmental impacts of the concrete mixes were compared using an MS Excel based Life-cycle Assessment (LCA) tool "GreenConcrete LCA" developed by the co-authors of this paper [23]. This cradle-to-gate LCA covers direct and supply-chain global warming potential (GWP) in units of CO_2-equivalent (CO_2-eq) emissions

and major criteria air pollutants (CO, NO_x, PM_{10}, and SO_2) associated with the use of electricity, fuel, transportation, and production processes taking place within the boundary of concrete production system. In LCA applications, drawing the system boundaries, i.e., decisions on inclusion or exclusion of processes in an analysis, is an essential step [24]. This study incorporates the following parameters in the system boundary: extraction of cement raw materials, manufacturing of cement, extraction and processing of aggregates, manufacturing of superplasticizers, preparation and treatment of fly ash prior to mixing in concrete, extraction and processing of limestone, and concrete batching and transportation of raw materials and products within the system.

2 Materials

For all the HVFA-L SCC trial mixes, the common goal was to reduce the cement content in order to minimize the environmental footprint while maintaining the required flowability specifications.

The powder materials used in the mixes are ASTM Type I/II portland cement (C), Class F Fly Ash (F), and ground limestone powder (L). Figure 1 shows volume-based particle size distributions of the powder materials obtained by laser light scattering. Table 1**Error! Reference source not found.** summarizes the particle size distribution data. The measured mean particle diameters were 10.4 µm, 22.2 µm, and 48.1 µm, respectively, for C, F and L. The D10, D50, and D90 values correspond to diameters at which the cumulative sample was under 10%, 50%, and 90%, respectively. In general, C and F had

much finer particle sizes when compared to L; however, F had some coarser particles of 25 μm and larger. The chemical compositions of powder materials are presented in Table 2.

X-ray powder diffraction (XRD) measurements on L and F used in this study were performed using a PANalytical X'Pert PRO Materials Research Diffractometer. Finely ground samples were loaded into metal sample holders and placed into the diffractometer. Data were collected using a cobalt target that produces X-rays with a wavelength of 1.789 Å. XRD patterns taken at ambient conditions are presented in **Error! Reference source not found.** Figure 2 together with schematic diagrams for relevant phases. The F measurement and the L measurement are plotted with the same intensity scales. Although the F is mainly composed highly amorphous aluminosilicate glass [25], the XRD analysis reveals that it also has several crystalline phases including mainly quartz (SiO_2), but also included hematite (Fe_2O_3), magnetite (Fe_3O_4), mullite ($3Al_2O_3{\cdot}SiO_2$), and anhydrite. The XRD analysis of L showed that it was composed mainly of calcite ($CaCO_3$) and dolomite [$CaMg(CO_3)_2$], and also included quartz, clinochlore, and muscovite. Similar phases were observed in fly ash [26] and limestone [26-28] samples by other researchers.

The fine aggregate used was a quartzitic sand (with fineness modulus 3.1); the coarse aggregate consisted of pea gravel (maximum size 12.7mm) and basalt (maximum size 19.0mm).

The only chemical admixture used was a carboxylated polyether-based high-range water reducer (ADVA 140) with a specific gravity of 1.010-1.120 in order to maintain the required workability. The chosen superplasticizer meets the requirements of ASTM C494 as Type A and Type F, and ASTM C1017 as Type I. Typical addition proportions were provided by the manufacturer as 0.65% to 1.14% by weight of cementitious materials as a high-range water reducer and 0.36% to 0.65% as a medium-range water reducer. The maximum suggested dosage was 1.43%. The dosage used for the trial mixes prepared in this study ranges from 1.00% and 1.43%. No viscosity-modifying admixture was used.

3 Experimental and analytical methods

3.1 Concrete mixture proportions

The concrete mixture proportions are shown in Table 3. The differences considered for mix selection were aggregate fractions, proportion of powder materials, and workability of concrete. The w/cm ratio was held constant at 0.35. For SCC mixes, typical aggregate-to-cementing materials ratio varies between 2:1 to 4:1 by weight [5]. To reduce overall cement content compared to typical SCCs, the total aggregate-to-cementing materials ratio was experimentally set at 4:1. The ratio of portland cement replacement (CR) to F and L was varied between 45–75% by weight. For the ternary blends (C-F-L), L content was fixed either at 15% by weight or 25% by weight; the amount of fly ash varied between 20-60% by weight in order to match the desired total replacement ratio for each mix. The ratio between coarse and fine aggregates was fixed at

50:50% by weight, and the coarse aggregate consisted of 30% by weight pea gravel and 70% by weight basalt.

The workability factor that satisfied SCC requirements was targeted and water-reducing admixture was added until the slump flow diameter was between 56-69 cm, and the flow time to achieve a diameter of 50 cm(T_{50}) was between 2-5 seconds.

3.2 Sample Preparation

A total volume of 22 liters of concrete was prepared in a pan planetary-type mixer for each mix. First, coarse aggregates and a small amount of water were mixed for 30 seconds. Then, cement, fly ash, and more water were added and mixed for 1 minute. Limestone powder and the rest of the water were added and mixed for 1 minute before the water reducer was added and mixed again for 1 minute. Fine aggregate was added and mixed for 3 minutes. During that time, the mixer was stopped if necessary, and the bottom of the mixer was scraped to remove fine particles.

Slump flow test was performed on the prepared mix (Section 2.4). When the concrete mix performed satisfactorily in regard to slump flow diameter and T_{50}, it was returned to the mixer and mixed for an additional minute before casting. If the slump flow time was too low or too high, the concrete was returned to the mixer, mixed for an additional minute and the water reducing admixture was adjusted until workability looked to be sufficient. Then the slump flow test was performed once more. If the concrete was then satisfactory in terms of consistency and workability, it was remixed for

an additional minute before casting. Otherwise, it was discarded and a new trial mix was prepared with a proper amount of water-reducer admixture.

Once the concrete mix was ready, it was cast into eighteen 75×150 mm cylinders and three 100×200 mm cylinders in two lifts without mechanical vibration. Light shaking was allowed as the only method of consolidation. Cylinders were immediately covered with plastic wrap and remained undisturbed for 24 hours at the ambient laboratory conditions. The cylinders were then demolded and placed in an environmental chamber at 100% relative humidity and room temperature (23±2°C) until testing in accordance with ASTM C 192 [29].

3.3 Experimental Procedures

Each mix was evaluated for normal consistency and setting time by testing the cement pastes, and slump flow, compressive strength, chloride penetration coefficient, water absorption, and gas permeability by testing concretes. The test results were used as basic indicators of workability, mechanical strength, and durability properties.

3.3.1 Normal consistency and setting time

The binary and ternary cement blends and control mixes were tested for normal consistency in accordance with ASTM C187 [30]. The cement pastes were proportioned and mixed to normal consistency, and thereafter the Vicat needle penetration test was conducted to obtain the initial and the final time of setting according to ASTM C191 [31].

3.3.2 Slump flow test

To assess the properties of the fresh concrete, the slump flow test was carried out according to ASTM C1611 [32]; and the flow diameter and T_{50} time was recorded. To evaluate for SCC characteristics, flow diameter and T_{50} were checked at 550–700 mm and 2–5 seconds, respectively [33-35]. In addition, segregation and bleeding were checked qualitatively by observing aggregate density and excess liquid near the slump flow perimeter.

3.3.3 Compressive strength test

Compressive strength of concrete was determined at 7, 28, and 91 days, and one year on 75×150 mm cylinders according to ASTM C39 [36]. The results reported present the mean values of three samples for each mix and curing period. Rubber pads were used to cap all 7-day samples and 14-day samples (ASTM C1231 [37]), while all others were capped with sulfur mortar (ASTM C617 [38]). The compressive strength of cylinders was measured under a stress rate control machine until significant softening was observed. The maximum load value was taken as the compressive strength. To keep the coefficient of variation (ratio of standard deviation to mean) less than 10% for each mix and curing period, the outliers were determined and removed from the data. The cylinder size was preferred for convenience and economy, yet testing 75×150 mm concrete cylinders with 19.0 mm maximum size aggregate undervalue compressive strength by 2.94%, compared

to the standard 100×150 mm concrete cylinders due to the "wall effect" [39, 40]. For that reason, the correction factor of 102.94% was used in compressive strength calculations.

3.3.4 Non-steady state chloride migration test

To determine the resistance of one-year-old concrete samples to chloride penetration, a non-steady state chloride migration test was performed in accordance with Nordtest Method, NT BUILD [41]. The 100×200 mm cylinder samples were sawed into 50 ± 2 mm-thick sections and cured in the fog room until the testing date.

Three specimens were tested for each mix. They were preconditioned by vacuuming in the saturated $Ca(OH)_2$ solution and then settled between a catholyte solution (10% NaCl) and an anolyte solution (0.3 N NaOH). The specimens were tested under a 30 V electrical potential for 24 hours. Each specimen was then split axially into two pieces, and a 0.1 M $AgNO_3$ solution sprayed on the freshly split surfaces where the areas containing chloride ions colored white. The chloride penetration depth was measured on photographic images of the specimens enlarged with image-processing software at seven points over 70 mm distance from the white silver chloride precipitation. From the mean penetration depth, the non-steady state chloride migration coefficient D_{nssm} (2) was calculated, as described in NT BUILD 492 [41], with:

$$D_{nssm} = \frac{0.0239(273+T)L}{(U-2)t} \cdot \left(x_d - 0.0238\sqrt{\frac{(273+T)Lx_d}{U-2}}\right) \qquad (1)$$

where

$$\square = \frac{\square - 2}{\square}$$

and

$$\square = 2\sqrt{\frac{\square\square\square}{\square\square\square\square\square}} \cdot \square\square\square\square^{-1}\left(1 - \frac{2\square}{\square_0}\right)$$

where D_{nssm} is the non-steady-state migration coefficient, m^2/s; z is the absolute value of ion valence for chloride, $z = 1$; F is the Faraday constant, $F = 9.648 \times 10^4$ J/(V·mol); U is the absolute value of the applied voltage, V; R is the gas constant, $R = 8.314$ J/(K·mol); T is the average value of the initial and final temperatures in the anolyte solution, K; L is the thickness of the specimen; x_d is the average value of the penetration depths, m; t is the test duration in seconds; erf^{-1} is the inverse of the error function; c_d is the chloride concentration at which the color of the concrete changes, c_d generally equals 0.07 N (N is the molar concentration divided by an equivalence factor) for OPC concrete; and c_0 is the chloride concentration in the catholyte solution, about 2 N. Three specimens were tested for each mix, and the average result was calculated.

3.3.5 Water absorption test

A water absorption test was carried out on the one-year-old concrete specimens, 100 mm in diameter and 50 mm in thickness, in accordance with the ASTM C948 [9]. The specimens were immersed in 21°C water and weighed every 24 hours until obtaining SSD weight stabilization, which requires less than 0.5% weight difference between two successive measurements. The last weight obtained of specimens was designated as *B*.

Then, the specimens were dried at 100–110 °C in oven, and weighed every 24 hours. Once a weight loss of less than 0.5% of previously measured weight was obtained, the specimen was cooled in a vacuum desiccator to room temperature. The weight of the specimen in room temperature was assigned as *C*. The water absorption is determined as follows:

$$\text{Water absorption (\%)} = \frac{B - A}{A} \times 100 \quad (2)$$

3.3.6 Gas permeability test

The gas permeability was performed on the one-year-old oven-dried specimens according to the CEMBUREAU method [42] to determine the gas permeability coefficient. Nitrogen gas was applied to the specimens at five particular gas pressures differing from 0.5 bar (0.05 MPa) to 2.5 bar (0.25 MPa) with an incremental of 0.5 bar (0.05 MPa). Flow times of nitrogen gas were recorded until a steady-state flow was obtained. The steady-state condition was reached once the difference between two successive flow times was less than 3% within 5 minutes. For each gas pressure stage, the gas permeability coefficient, K_g, was calculated using the Hagen-Poiseuille relationship for laminar flow of a compressible fluid through a porous medium under steady-state conditions [43], so that:

$$K_g = \frac{2 Q_0 P_0 \mu L}{A (P_1^2 - P_2^2)} \quad (3)$$

where K_g is the gas permeability coefficient (m^2); Q is the volume flow rate of the fluid ($m^3\ s^{-1}$); A is the cross-sectional area of the specimen (m^2); L is the thickness of the specimen in the direction of flow (m); μ is the dynamic viscosity of the nitrogen at test temperature ($N\ s\ m^{-2}$); P is the inlet (applied) pressure (absolute) ($N\ m^{-2}$); P_a is the outlet pressure assumed in this test to be equal to atmospheric pressure ($N\ m^{-2}$); and P_0 is the pressure at which the volume flow rate is determined, assumed in this test to be atmospheric pressure ($N\ m^{-2}$).

3.4 Analytical procedures

A life-cycle approach systematically studies the environmental impacts of concrete by the quantification of resource inputs and environmental burdens (life-cycle inventory compilation), and estimates the impacts of these inputs and burdens on humans and nature (impact analysis), and identifies areas where improvements are possible. Therefore, LCA is particularly crucial for a methodical analysis of the cradle-to-gate environmental impacts of concrete production given the high volumes of concrete use, the growing importance of environmentally sustainable infrastructure decisions, and the fact that once concrete is put in a structure certain environmental factors are static for many years [44].

3.4.1 LCA methodology

The LCA approach is a methodological framework that assesses the environmental impacts and resources (including raw materials, energy, etc.) used throughout a product's

life-cycle from raw material acquisition through production, use, maintenance, recycling, and ultimate disposal. ISO 14040 series are accepted as providing a consensus framework, terminology, and some methodological choices for performing a LCA [45, 46]. The LCA consists of four major stages, as illustrated in Figure 3.

The goal and scope definition of an LCA provides a description of the product system in terms of the system boundary and functional unit. The functional unit, measured in the cubic meter of ready-mixed concrete, is the basis for comparison throughout the study [45-47]. In the GreenConcrete LCA tool, the system boundary starts with the extraction of cement and concrete raw materials, and covers major material production and preparation processes (e.g., cement, aggregates, admixtures, fly ash, and limestone), transportation of materials within the system, mixing of concrete materials at the batching plant, and ends at the gate of the concrete plant with the final product being the concrete mixture ready to be used at the construction site.

The life-cycle inventory (LCI) stage estimates the consumption of resources and quantities of waste flows and emissions caused by or otherwise attributable to a product's life-cycle. The processes within the life-cycle and associated material and energy flows as well as other exchanges represent the product system and its total inputs and outputs from and to the natural environment, respectively. Within the scope of the study, authors of this study estimate GWP (in CO_2-eq) as well as major criteria air pollutants that include CO, NO_X, PM_{10}, and SO_2.

The life-cycle impact assessment (LCIA) stage evaluates the potential human and ecological effects of energy, water, and material consumption and the environmental releases identified in the inventory analysis. This stage involves classification, characterization, and normalization of impact categories. For the purpose of this study, concrete production GWP, that is relative to that of 1 kg of the reference gas CO_2 (in CO_2-eq) is calculated based on IPPC guidelines as follows [48, 49]:

$$GWP_{100_{YEAR}} = 1 \times CO_2 + 21 \times CH_4 + 310 \times N_2O$$

The life-cycle interpretation is the last stage of the LCA process. It is a systematic technique to "identify, quantify, check, and evaluate information from the results of the LCI and the LCIA, and communicate them effectively" [24, 46, 50, 51]. Results from the GreenConcrete LCA are discussed as part of the interpretation stage in following sections.

3.4.2 Environmental assessment of concrete mixtures

This study used a concrete production LCA tool named as GreenConcrete LCA [23] to assess the environmental profiles of concrete mixes. The tool evaluates both direct and supply-chain environmental impacts of each process during the production of concrete and concrete-making materials. For example, when a process involves the use of electricity, the tool provides not only direct electricity generation impacts but also supply-chain impacts that encompass the construction and operation of a power plant, as well as the life-cycle impacts of the major resources used in the construction of the plant,

the operation of the plant, and so on. Moreover, integration of regional variations and technological alternatives in the material production processes within the tool offers a wide range of applicability and flexibility for cement and concrete manufacturers in the United States and worldwide.

Table 4 and Table 5 summarize the LCA inputs used in the GreenConcrete LCA tool regarding the production technologies, geographic locations, electricity grid mix percentages, transportation distance and mode selection, as well as type of material choices , based on a real case scenario.

4 Results and Discussion

4.1 Normal consistency and setting time

Water to cementitious material ratios desired for normal consistency and initial and final times of setting of cement blends are shown in Table 6 and Figure 4. Water demand of *C70-F30* and *C50-F50* was 8% and 12% lower than that of control *C100*, respectively. The ternary *C25-F60-L15* blends showed 19% less water demand than the control *C85-L15*. This indicates that addition of F in the cement system greatly decreased the water demand in cement paste. In general, the more L in the cement blends requires slightly more w/cm for the normal consistency. The water demand of *C45-F30-L25*, for instance, was approximately 5% higher than that of *C45-F40-L15*.

Error! Reference source not found. Figure 4 shows that changing the mix proportions of F and L had a strong influence on the initial and final times of setting. Binary and ternary blends showed longer setting times compared to the control specimens. The larger amounts of cement replacement with F elevate the initial and final setting times in both of the binary and ternary cement systems. Significantly, the final setting times of *C70-F30* and *C50-F50* were about 1.4 and 2.3 times longer than the control *C100*. When the F30 mixes are compared, the *C70-F30* had much lower initial and final setting times than the *C55-F30-L15* and *C45-F30-L25*. However, when compared to *C50-F50*, the cement replacement with L in ternary mixes lowered the setting times. For example, the final setting time of *C45-F40-L15* and *C 45-F 30-L25* was almost 18% and 29% shorter than that of *C50-F50*, respectively.

4.2 Fresh concrete flowability

The slump flow diameter (d_s) and T_{50} times of the concrete mixtures are presented in Table 7. According to the slump flow results, all mixes met the specified SCC requirements; see Table 8 [52]. The visual stability index (VSI) values of the mixes were evaluated between zero and one: zero shows no evidence of segregation or bleeding, and one showed segregation and slight bleeding as a sheen on the concrete mass, in accordance with ASTM C1611 [32]. Due the constant water content and variable use of water reducing agent, the impact of F and L replacement on flowability is not clearly discernible. However, it was noted that generally the necessary water-reducer content,

and T_{50} decreased, or d_s increased with the addition of fly ash to the mixes (Table 7). Notably, the *100C* control concrete had a lower flow diameter and higher flow times, as compared with the more workable *50C–50F* concrete, even though the amount of water reducer used in the *100C* concrete was 25% greater.

4.3 Compressive strength

Table 9 presents the average compressive strength for all concrete mixtures, while Figure 5 shows the results in graphic form. As can be readily observed in this figure, a wide range of strengths are attainable depending on the specific replacement ratios and curing time specified for a given project. Similarly, a given strength can be obtained using a variety of mixes and cement replacement ratios. For example, a strength level of 30 MPa can be obtained either at 28 days with a total cement replacement level of up to 55% (either using 15% L+ 40% F or 25% L + 30% F), or at 56 days with a replacement level of up to 65%, or at 91 days with a cement replacement level as high as 75%. Higher strengths can also be easily achieved. The 45% replacement mix with 30% F and 15% L reached approximately 42 MPa at 28 days, growing to about 54 MPa at 91 days.

The early age data is very similar for the 15% L and 25% L series. At 7 days, F-L mixes ranged between 9 MPa for 75% replacement and 20 MPa for 45%. At 28 days, these mixes reached 19 MPa for 75% replacement and approximately 40 MPa for 45%. At 56 days, this range was 24 MPa to 44 MPa. Finally, at 90 days the F-L mixes obtained a minimum of 31 MPa and up to 54 MPa for the 30-15 mix.

As expected, at a fixed w/cm ratio as used herein, increased F content led to relatively lower early strengths but higher strength gain rates, as shown in Figure 5**Error! Reference source not found.**, which plots σ_c against time.

Note the remarkable synergistic effect between limestone powder and fly ash shown in Figure 5 **Error! Reference source not found.**(a) and (b) compared to the control mixes, shown in Figure 5**Error! Reference source not found.** (c), in which the addition of fly ash led to reduced compressive strength. In several cases, the compressive strength actually increased for the limestone series mixtures when portland cement was replaced by fly ash up to a certain amount. For the 25% limestone series with 20% fly ash (45% total replacement ratio), at 28 days the strength was 8% higher than the zero fly ash mix (with only 25% replacement); the strength was kept increasing over time. With 30% fly ash in both cases (15% and 25% limestone powder), the strength was only slightly lower than the zero fly ash mixes at 28 days, and it exceeded them at 56 days. At one year the strength of *55C-30F-15L* was slightly higher than the one of *85C-15L*. This suggests that the more sustainable product can be obtained with more cement replacement by fly ash. Investigating the influence of fine additives on the viscosity of cement paste, Diamantonis et al [53] also observed a synergistic effect in a mixture with 20% limestone powder and 20% fly ash. The authors concluded that the synergy between the materials can lead to a higher packing density that in turn results in a denser microstructure - a hypothesis which is also supported by Liu and Yan [34].

4.4 Durability assessment

4.4.1 Coefficient of chloride migration

Error! Reference source not found. Figure 6a demonstrates that the mixing ratio of F and F–L as a cement replacement had a strong effect on the chloride migration coefficient of the experimental concretes. All the concretes with blended cement mixes demonstrated a higher resistance to chloride migration relative to the *100C* and *85C–15L* and *75C–25L*. Based on standard guidelines [54], the chloride penetration resistance of the C–F binary mixes and C-F-L ternary mixes ranged from extremely high to very high (Table 10). This result suggests that hydration of F and L impedes voids and pores, leading to pore size reduction and smaller effective chloride diffusivity.

The *50C–50F* showed higher resistance to chloride penetration than the 70C–30F. This suggests that the more the F replacement, the more chloride penetration resistance for the binary mixes. However, the *35C-50F–15L* showed lower resistance to chloride penetration than the *45C-40F–15L*, whereas the *45C-40F–15L* presented higher resistance to chloride penetration than *55C-30F –15L*. This indicates that more than 55% replacement for the ternary mixes lowers the resistance to chloride migration.

Significantly, for the same ratio of cement replacement with F and L, the ternary *35C-40F-25L* mix results in higher chloride migration *35C-50F-15L* mix. This indicates that the 25% L replacement in ternary blends had the added advantage of improving chloride resistance.

4.4.2 Water Absorption

Error! Reference source not found. Figure 6b shows that alterations in the cement replacement mixtures have a strong influence on the water absorption of the experimental concretes. The *70C–30F* and *50C–50F* binary mixes displayed lower water absorption compared to the control mixes and ternary mixes due to possible lower porosity. For the control specimens and ternary blends, the more L replacement resulted in more water absorption, with the exception of the *55C-20F-25L* which had lower absorption than the *55C-30F-15L*. In general, by the increasing the ratio of F replacement resulted in the higher water absorption in the binary and ternary mixes.

4.4.3 Gas Permeability

Error! Reference source not found. Figure 6c indicates that F and F–L mixes had a strong influence on the coefficient of gas permeability in the experimental concretes. Greater amounts of cement replacement with F lower the gas permeability in both the binary and ternary cement systems, with the exception of the *45C–40F–15L* and *35C–40F–25L* mixes. Adding L acts to increase the gas permeability with the exception of the *45C–30F–25L* that has 10% lower gas permeability than the *45C–40F–15L*; note that gas permeability is affected by drying procedure [52, 55-57]. Although there is a correlation between resistance to chloride penetration and gas permeability of concrete subjected to short-term air or oven drying, this correlation weakens with longer drying periods [58]. This is demonstrated for the specimens tested here with the CEMBUREAU method: even

though increasing F replacement of C in the binary and ternary mixes generally decreased gas permeability, it increased the chloride penetration coefficient for the 50% and more F replacement in ternary blends, which is the more straightforward measurement. Long-term drying in the gas permeability tests may have introduced artifacts into the specimens that obscure the meaning of the experimental results. Thus, microcracks induced in the concrete during longer drying periods may result in higher gas permeability in specimens with less OPC replacement [35, 52, 55-58].

4.5 Environmental Factors

Estimated GWP (in CO_2-eq) and criteria air pollutants associated with each concrete mix is illustrated in Table 11Table . Calculations for environmental interventions are obtained from the GreenConcrete LCA tool based on assumptions presented in Table 4 **Error! Reference source not found.** and Table 5.

For comparison purposes, typical ordinary portland cement (OPC) concrete having a 28-day strength of 18, 30, and 60 MPa (low-strength, medium-strength, and high-strength, respectively) cause emissions of 218, 304 and 436 kg CO_2/m^3, respectively. Based on these data, all self-consolidating F-L mixes have a lower cement content, and, therefore, a reduced $CO_{2\text{-eq}}$ footprint than even the low-strength OPC concrete.

These estimates can be compared to typical SCC mixtures obtained from the literature [18, 19, 59, 60]. An example SCC, which used 30% silica fume (SF) and 10%

F, would result in higher carbon dioxide emissions compared to typical concrete mixes. Because of the high volumes of SCMs in the mix, it has similar estimated $CO_{2\text{-eq}}$ emissions (299 kg CO_2/m^3) compared to medium strength OPC concrete. This is still higher than the F-L SCCs studied herein; Figure 7 demonstrates**Error! Reference source not found.** strength versus GWP trends for the mixes and compares average compressive strength (MPa) of the concrete mixes over time (days). Red line shows the calculated total GWP for concrete production (kg $CO_{2\text{-eq}}$ / m^3 of concrete); and the blue line shows the contribution of the portland cement used in the mixes to the GWP. Accordingly, GWP increases with the quantity of portland cement used in concrete mix. Figure 8 shows the calculated intensity of CO_2-eq emissions per unit volume of concrete per 365-day compressive strength versus 365-day compressive strength for the concrete mixes used in the study. The CO_2-eq intensity is considered as a better alternative of measuring the impacts of concrete use [61] because this indicator allows for the consideration of both performance (e.g., compressive strength) and contribution of concrete mixes to GWP per its unit volume and strength. For a given strength, lower CO_2-eq intensities are achieved by portland cement replacement with SCMs as observed in Figure 8. For example, at about 53 MPa strength, a 85% PC – 15% limestone powder concrete mix produces a 9.2 kg CO_2-eq.m^{-3}/MPa while a 55% PC – 20% fly ash – 25% limestone powder mix has a considerably lower intensity, that is 6.1 kg CO_2-eq.m^{-3}/MPa. Therefore, for a given performance measure, with improvements in mix design as well as

selection of materials, it is possible to reduce the carbon dioxide intensity of concrete mixes.

As shown in Table 11 Table and similar to GWP, all criteria air pollutants increase with amount of increase in portland cement, mostly because of fuel combustion during pyro-processing. The CO emissions are the only exception, which are slightly higher for concrete mixes with higher fly ash content (see the rate of change of CO emissions for mixes with higher fly ash content in Column 4 of Table 11Table). This is attributable to the natural gas with comparably higher CO emission factor used for drying the fly ash.

The GWP by major concrete ingredients were investigated in further detail; see Figures 9 to 12. In Figure 9, the total GWP for each of the concrete mixes involve direct and supply-chain emissions from all the quarrying, production, and transportation processes taking place in the system boundary. With a total of 569 kg of CO_2-eq, the concrete mix with 100% by weight portland cement (which is responsible from about 93% of the total) causes the highest amount of GWP (see Figure 9 and Figure 10**Error! Reference source not found.**). With the decreasing amount of portland cement and increasing amount of SCM, e.g., for 60F-15L mix, GWP from portland cement can be as low as 69% of the total concrete production. Transportation of materials to the concrete batching plant is the second highest source of emissions, affecting between 418% of the total depending on the amount of materials conveyed and transportation distance and mode (see Figure 11**Error! Reference source not found.**).

5. Conclusions

1. Without the use of any viscosity modifying admixtures, self-consolidating concrete mixtures can be produced with cement, high-volume fly ash, limestone powder, high ratio of the aggregate to cementing powders, and a low dose of superplasticisers.
2. A wide range of early and long term strengths were attainable depending on the selected mix proportion. The rate of strength gain increased with increasing fly ash content, and it was observed that for 25% limestone powder, the mix with 20% fly ash exceeded the strength of the control mix that contains only 25% limestone powder by 28 days. The mix with 30% fly ash performed similarly but by 91 days. This means that the synergistic effect between limestone powder and fly ash leads strength gain by the time of curing.
3. Similar but less pronounced the rate of strength gain was observed either with 15% limestone and fly ash mixtures or zero limestone and fly ash mixtures.
4. Concrete mixtures with 50% or less supplementary cementing materials attained 30 MPa compressive strength by 28 days, and all concrete mixes attained 30 MPa by 91 days.
5. The binary and ternary mixes with fly ash or fly ash and limestone powder were resulted in higher resistance to chloride penetration compared to 100C, 85C-15L, and 75C-25L control mixes. The binary mixes and ternary mixes with 25% L produced lower water absorption capacity than the reference mixtures of 100C and

75C-25L, respectively. However, the greater than 45% fly ash and L addition in the ternary mixes that contains 15% L demonstrated higher water absorption than 85C-15L control mix.

It is worth to note that an additional benefit of using large amount of supplementary cementitious materials in the reduction of heat of hydration [62] is not tested in this study. The reduction of heat of hydration could be resulted in higher strength and durability performance for concrete with high-cement content and concrete members with large size (i.e., foundations, piers, and dams).

6. Greenhouse gas (GHG) emissions and major criteria air pollutants were also successfully reduced and were in all cases similar to and lower than typical ordinary portland cement concrete. The only exception to this was CO emissions, which were estimated to be slightly higher for mixes with higher with fly ash content due to use of natural gas in drying the fly ash prior to use in concrete). Regarding the GHG emissions from other non-cementitious ingredients, Figure 10 demonstrate that their mass contribution remains almost constant for all mixes: about 4 kg for fine aggregates (1–2%), 4-5 kg for superplasticizers (1–2%), 3 kg for coarse aggregates (1%), and 1.5 kg for concrete mixing and batching activities (0.3–1%). Finally, Figure 11**Error! Reference source not found.** summarizes the GWP from limestone production and fly ash preparation, which can be as high as 3% in total for the mix with the highest cement replacement content, e.g., 60F–15L

mix. The GWP from fly ash is found to be greater, on the order of 5–10 for the same weight of limestone used in the mix. This difference can be explained by the higher amount of fuel utilized per unit mass of fly ash during the drying process as part of treatment prior to mixing in the concrete [63].

Figures

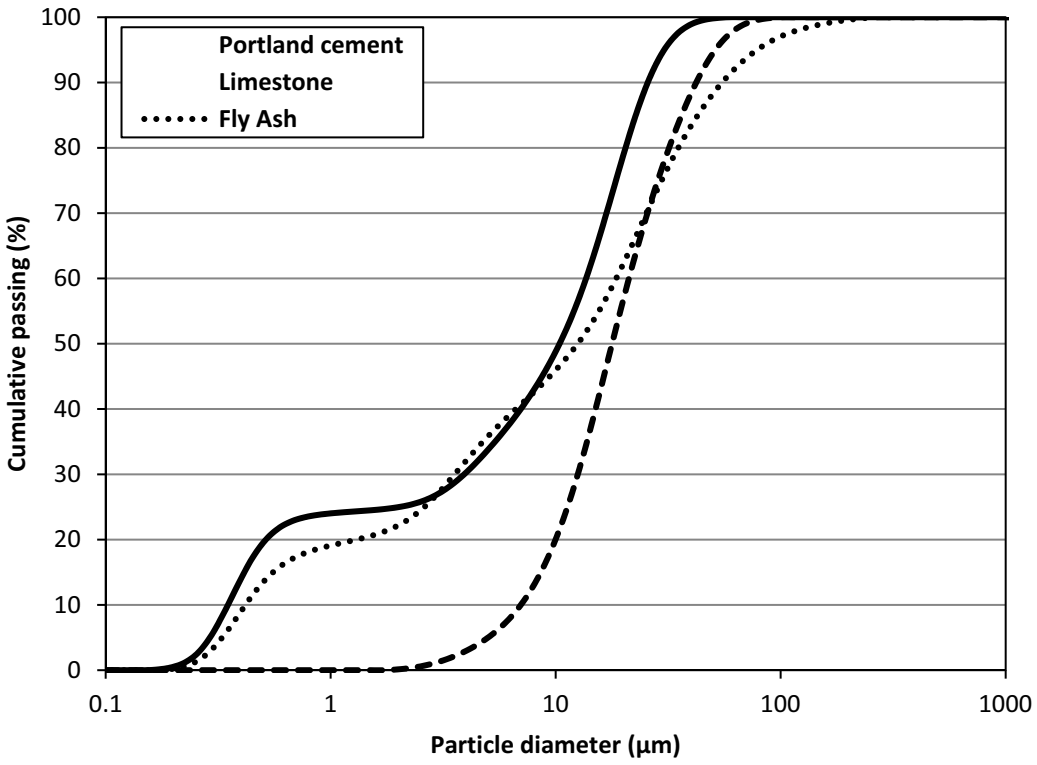

Figure 1. Particle size distributions of portland cement (C), limestone powder (L) and Class F fly ash (F).

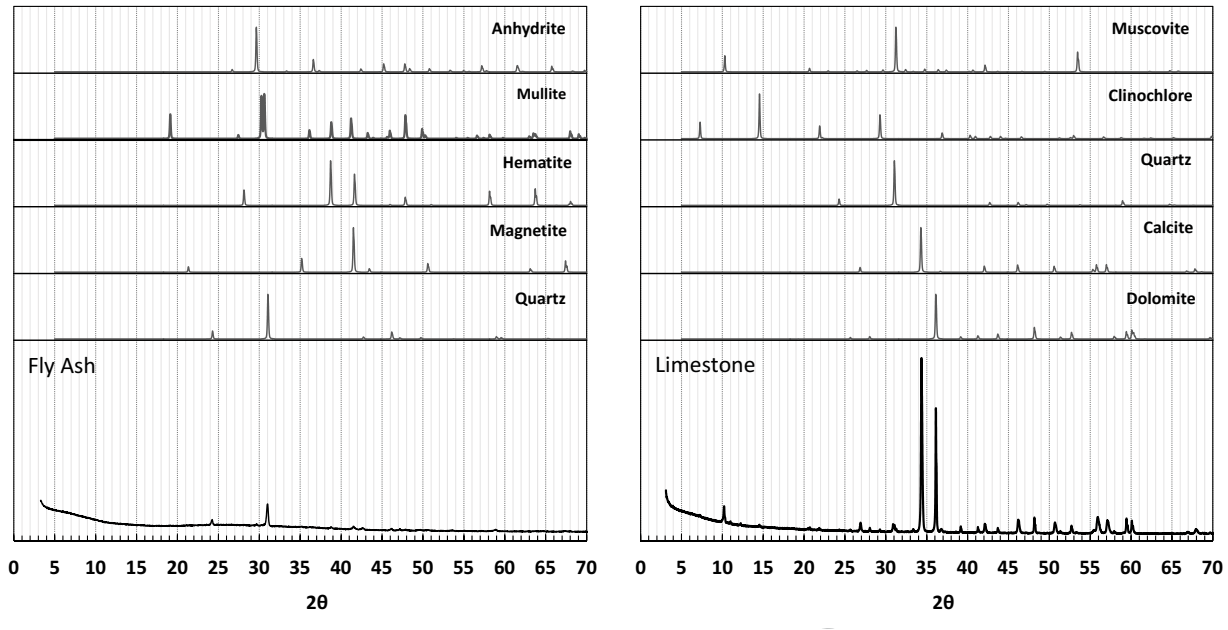

Figure 2. X-ray diffraction (XRD) patterns of the limestone powder (L) and the class F fly ash (F).

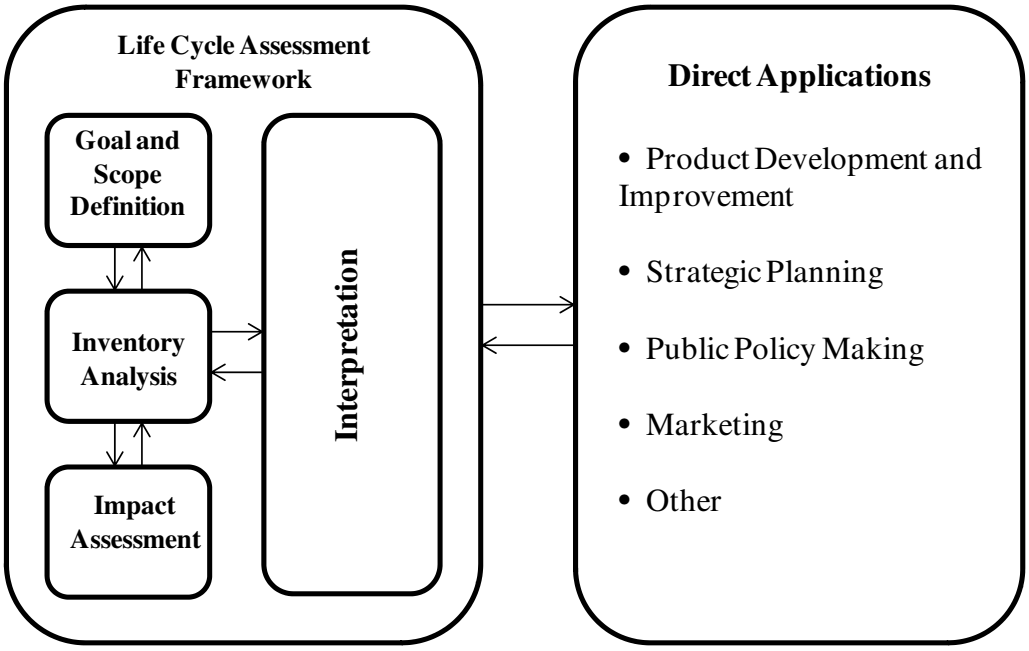

Figure 3. Stages and applications of an LCA, adapted from [46, 50, 64]

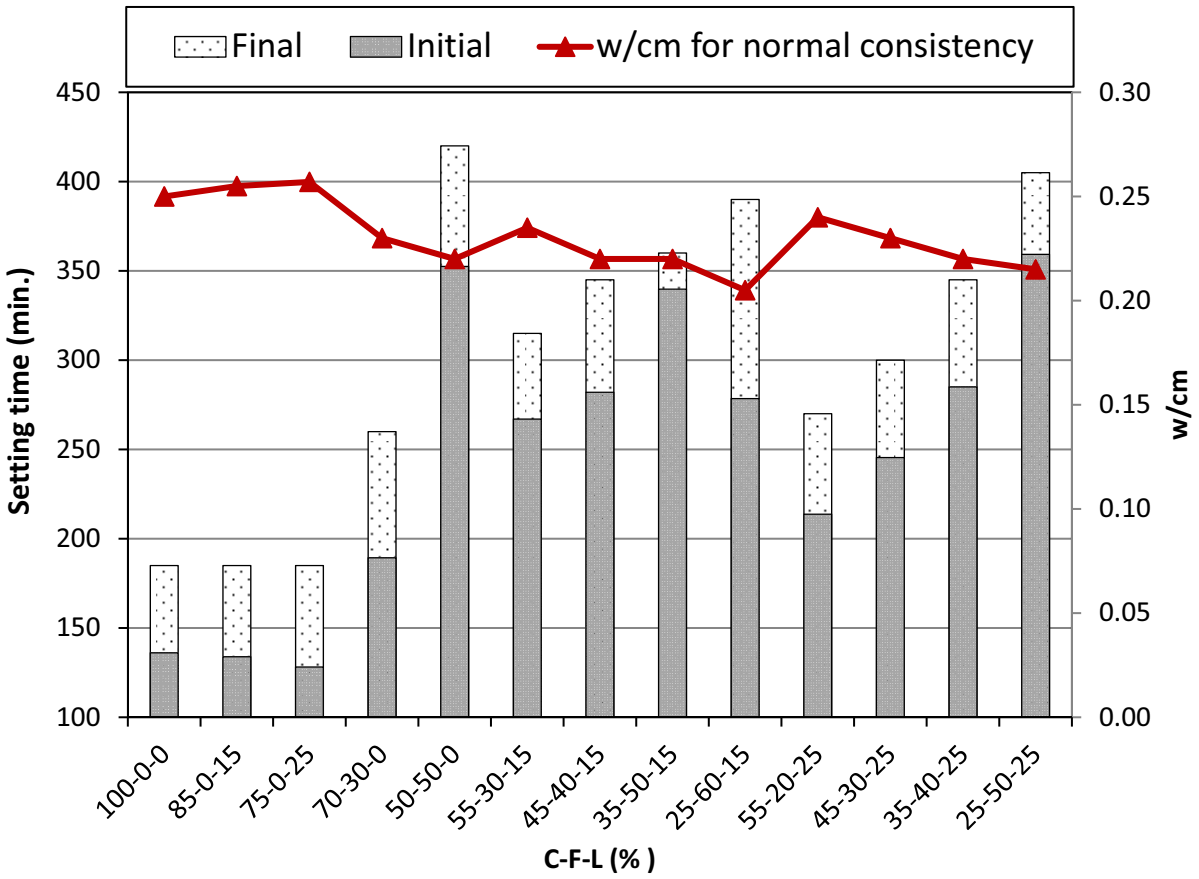

Figure 4. w/cm for normal consistency, and initial and final times of setting of the cement blends

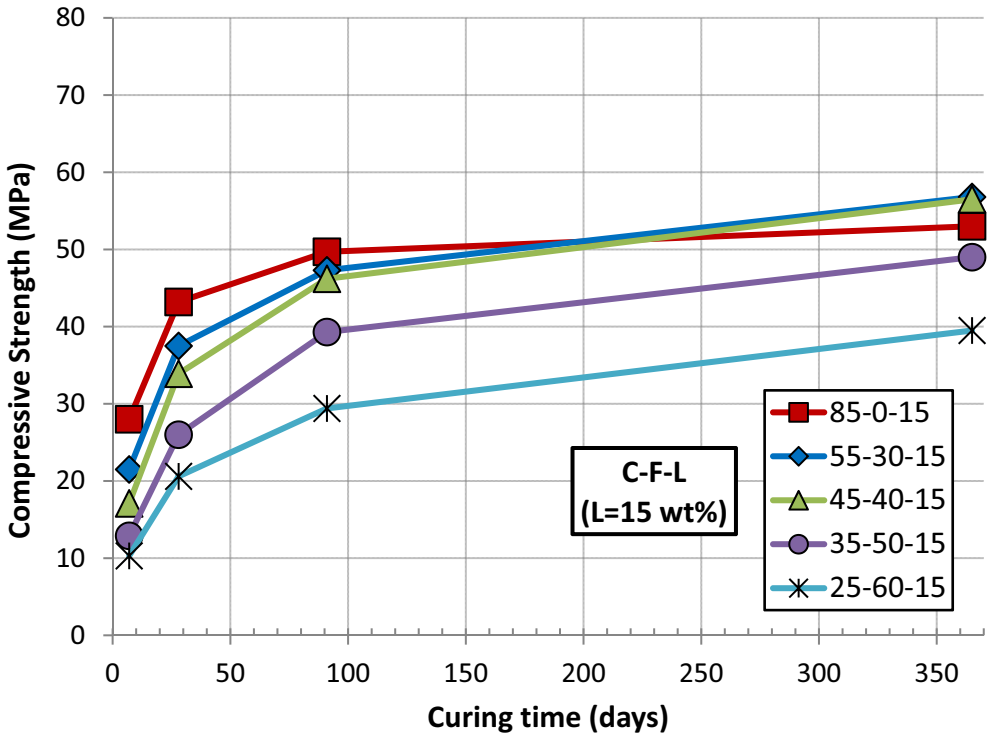
Compressive Strength (MPa)
Curing time (days)
C-F-L
(L=15 wt%)
85-0-15
55-30-15
45-40-15
35-50-15
25-60-15

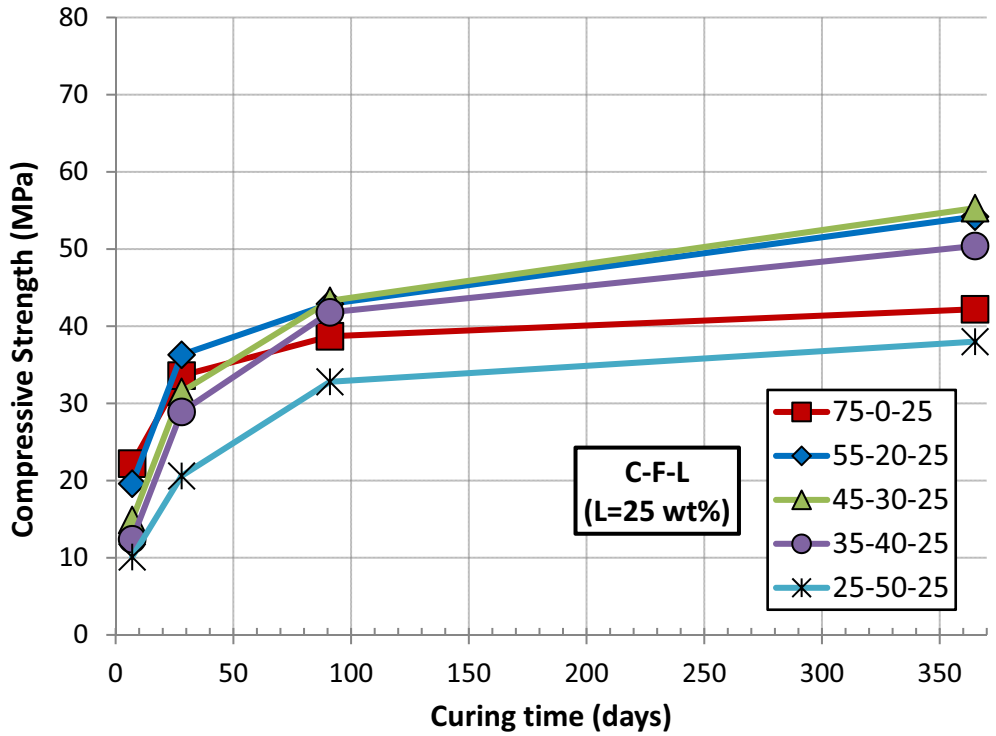
Compressive Strength (MPa)
Curing time (days)
C-F-L
(L=25 wt%)
75-0-25
55-20-25
45-30-25
35-40-25
25-50-25

5 (b)

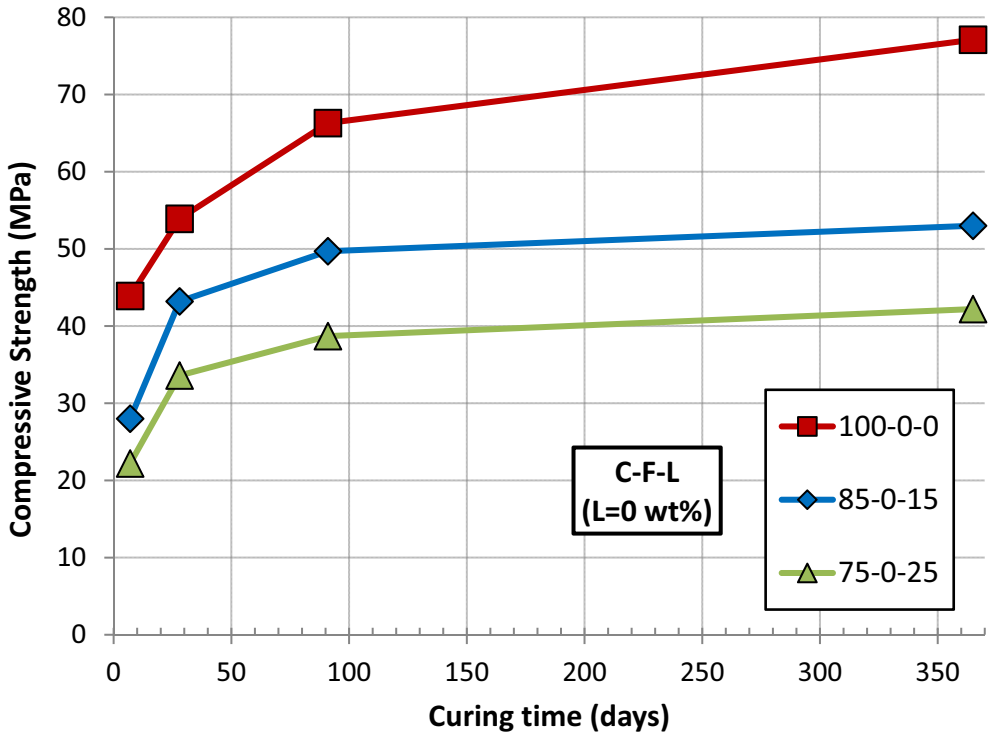

5 (c)

Figure 5. Compressive strength development over time (days). (a) 15% limestone series, (b) 25% limestone series, and (c) control mixes. Mixes with higher F content gain strength steadily over time, as expected.

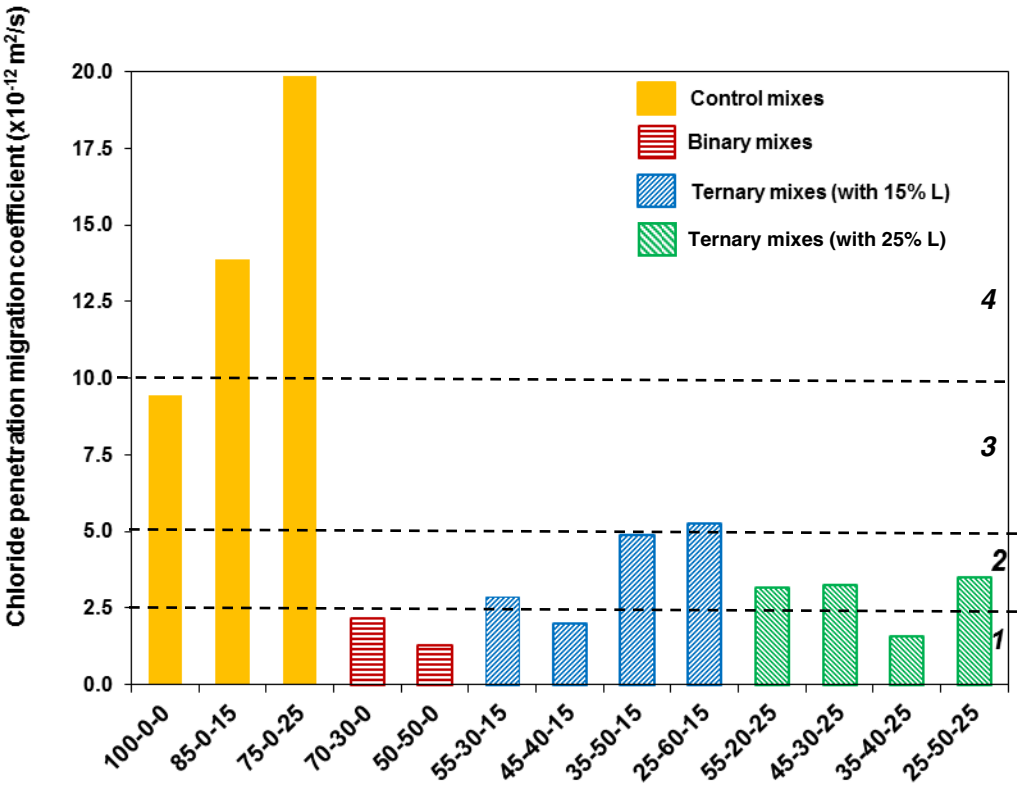
Chloride penetration migration coefficient (x10-12 m2/s)
20.0
17.5
15.0
12.5
10.0
7.5
5.0
2.5
0.0
Control mixes
Binary mixes
Ternary mixes (with 15% L)
Ternary mixes (with 25% L)
4
3
2
1
100-0-0
85-0-15
75-0-25
70-30-0
50-50-0
55-30-15
45-40-15
35-50-15
25-60-15
55-20-25
45-30-25
35-40-25
25-50-25

6 (a)

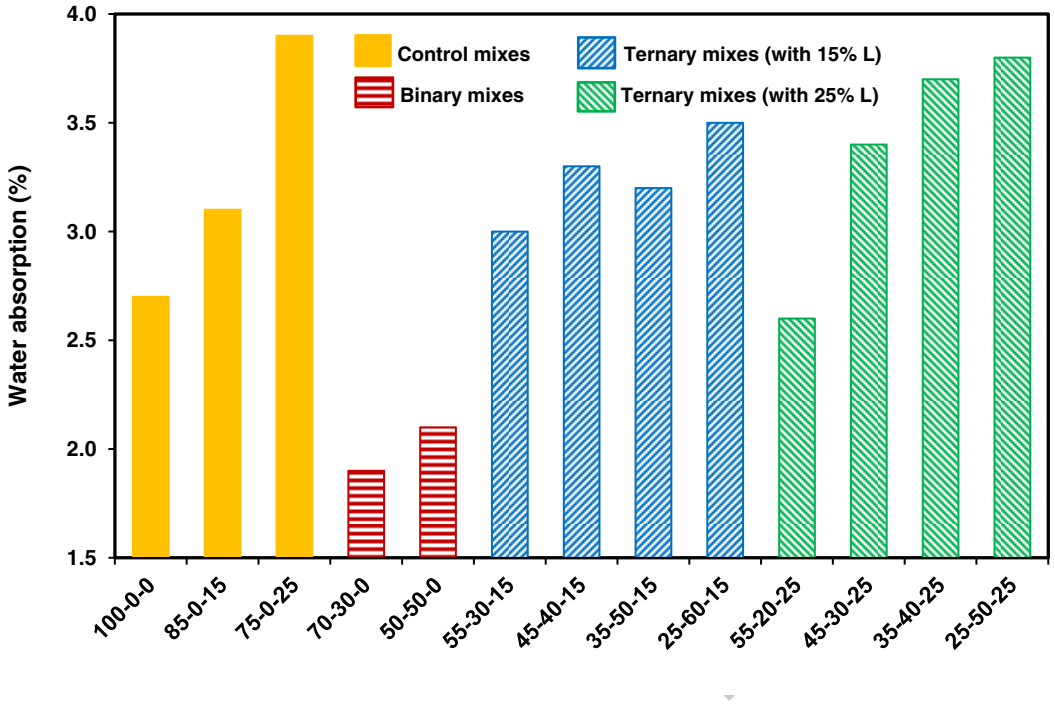
Water absorption (%)
4.0
3.5
3.0
2.5
2.0
1.5
Control mixes
Binary mixes
Ternary mixes (with 15% L)
Ternary mixes (with 25% L)
100-0-0
85-0-15
75-0-25
70-30-0
50-50-0
55-30-15
45-40-15
35-50-15
25-60-15
55-20-25
45-30-25
35-40-25
25-50-25

6 (b)

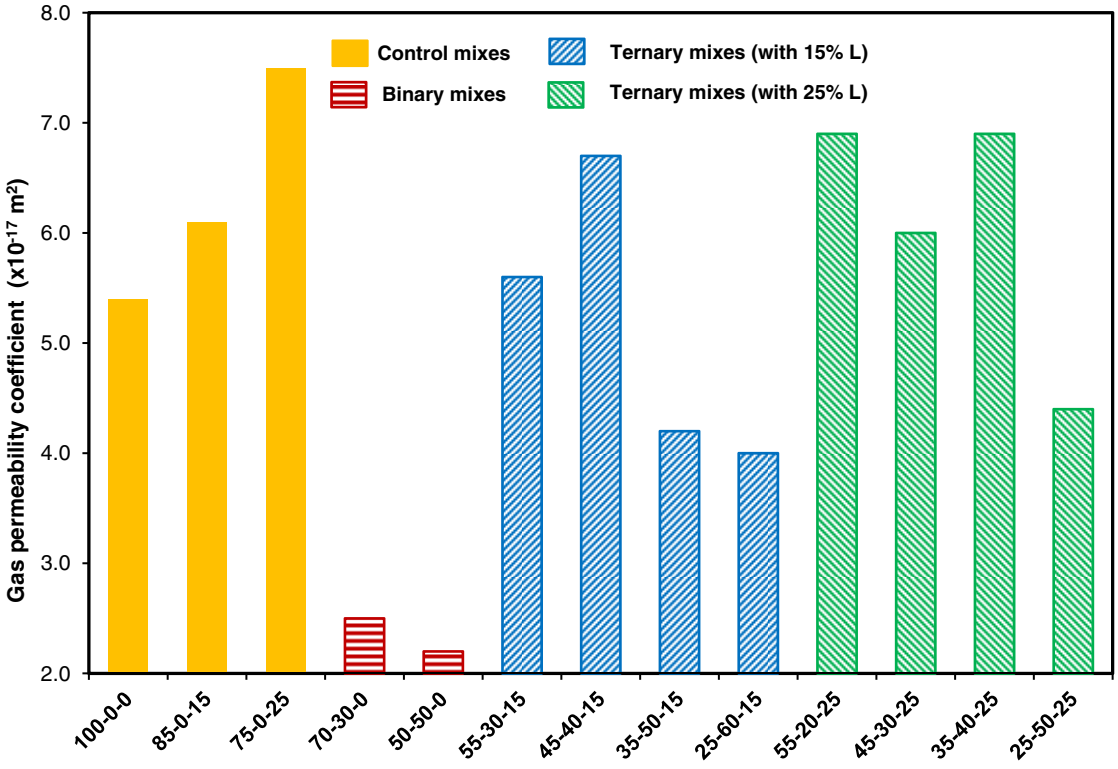

6 (c)

Figure 6. Results of durability tests of the experimental C–F- L concretes: (a) non-steady state chloride migration coefficient as a function of cement replacement of the concrete mix. Zones 1, 2, 3 and 4 indicate extremely high to moderate resistance to chloride penetration (Table 10); (b) relationship between water absorption and cement replacement; and (c) gas permeability coefficient in function of cement replacement of the concrete mix. All ratios listed as wt% C-F-L.

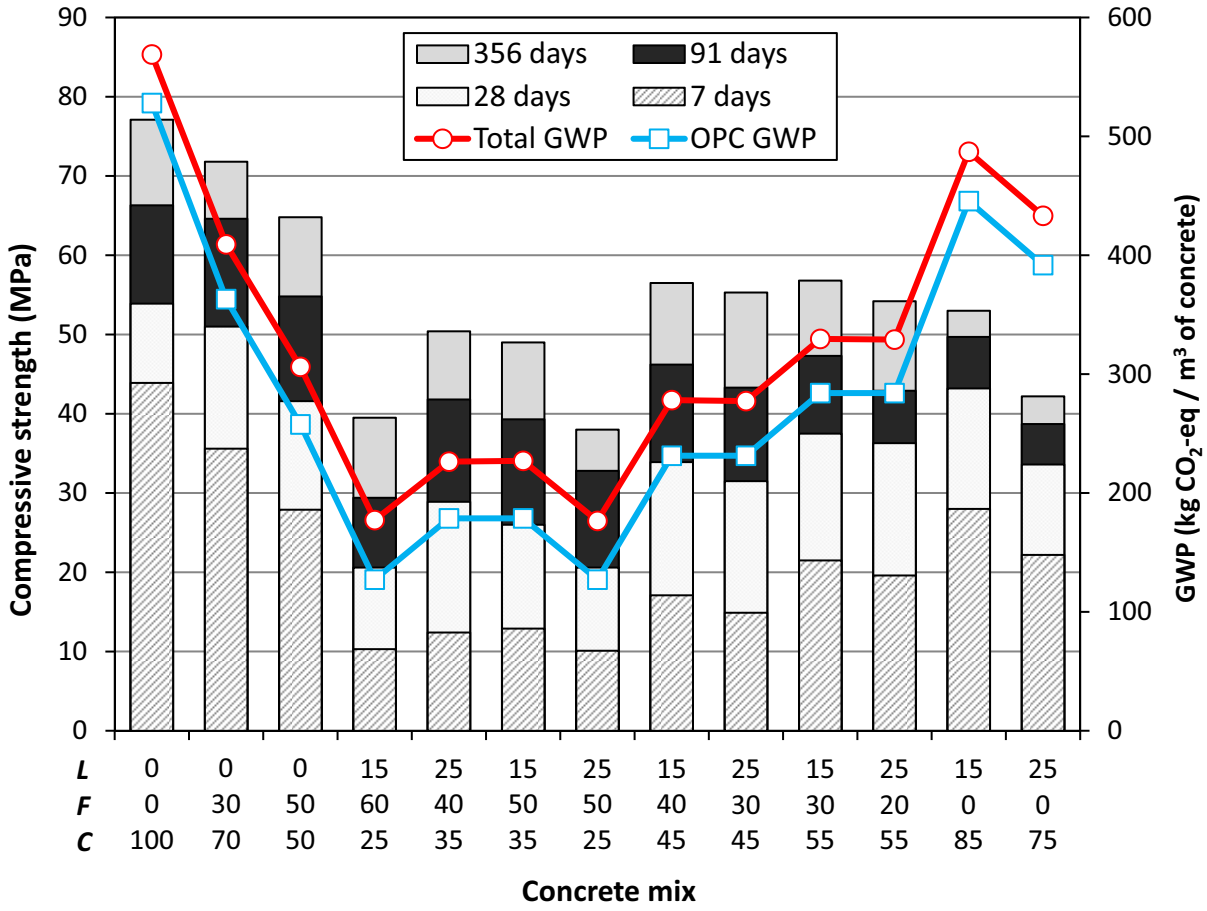

Figure 7. Comparison of average compressive strength (MPa) of the concrete mixes over time (days). Red line shows the calculated total global warming potential for concrete production (kg CO_2-eq / m^3 of concrete); and the blue line shows the contribution of the portland cement used in the mixes to the GWP.

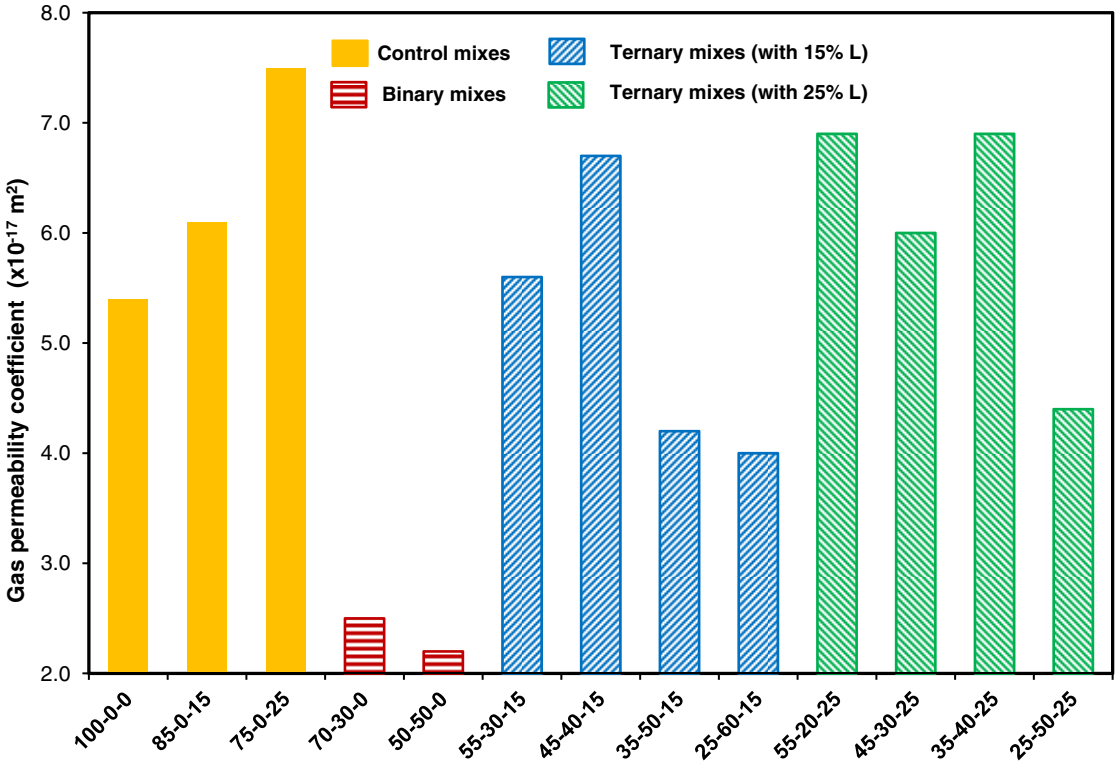

6 (c)

Figure 6. Results of durability tests of the experimental C–F- L concretes: (a) non-steady state chloride migration coefficient as a function of cement replacement of the concrete mix. Zones 1, 2, 3 and 4 indicate extremely high to moderate resistance to chloride penetration (Table 10); (b) relationship between water absorption and cement replacement; and (c) gas permeability coefficient in function of cement replacement of the concrete mix. All ratios listed as wt% C-F-L.

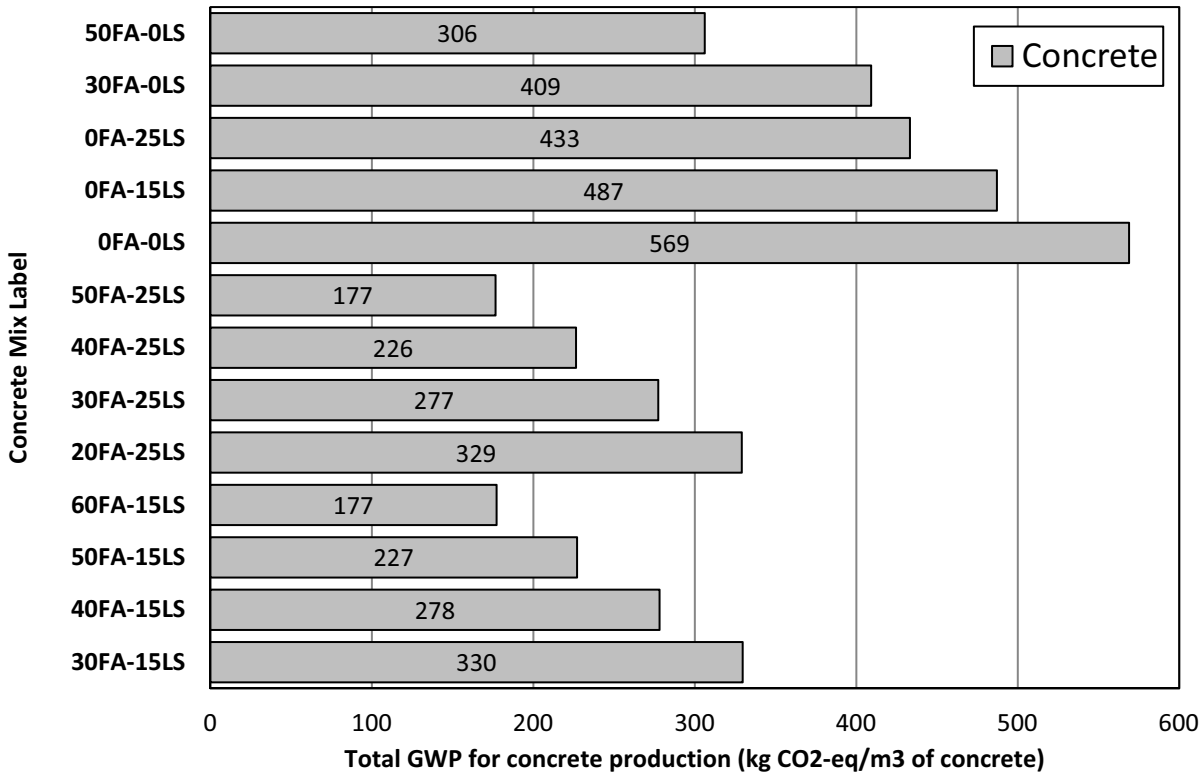

Figure 9. **Total GWP during concrete production (kg CO_2-eq / m^3 of concrete)**

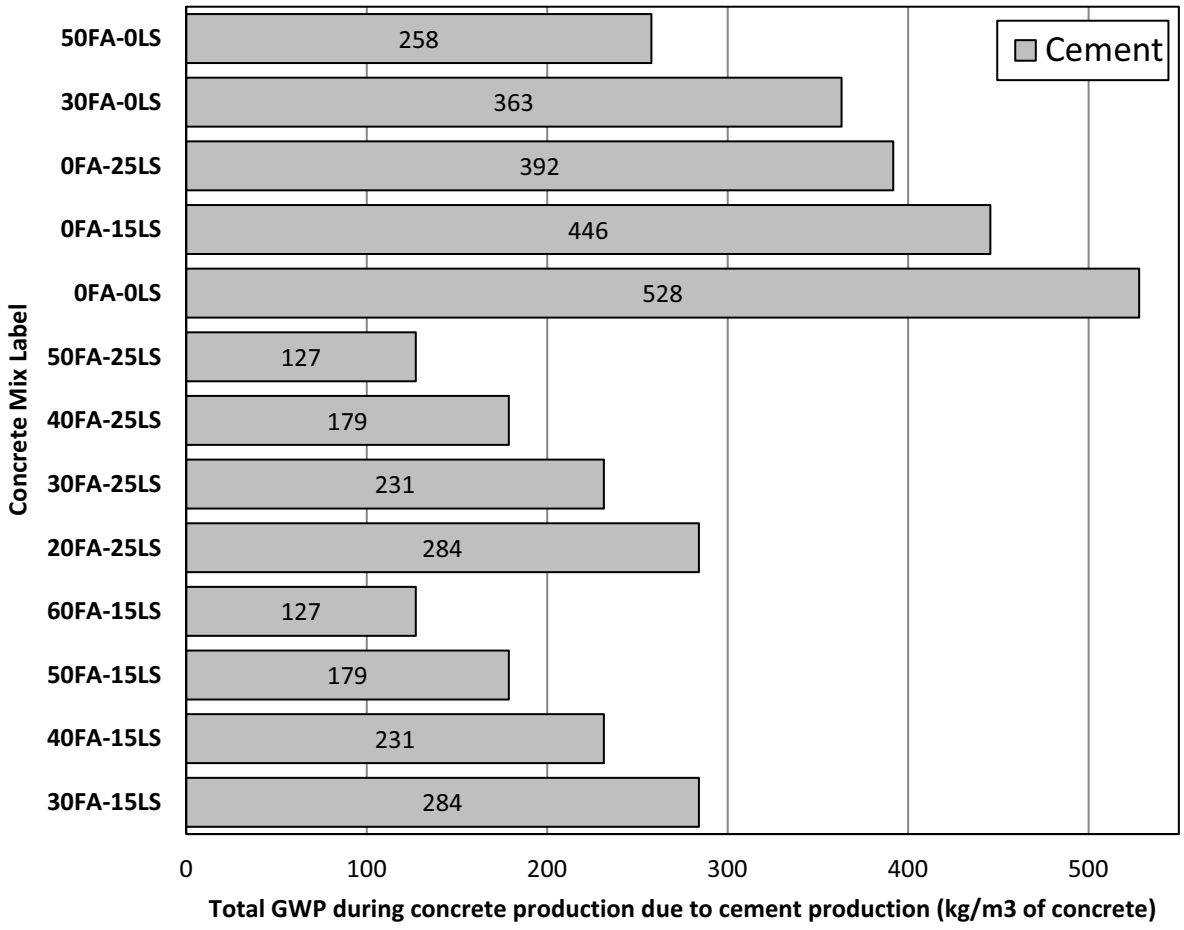

Figure 10. Total GWP associated with cement production only (kg CO_2-eq / m^3 of concrete)

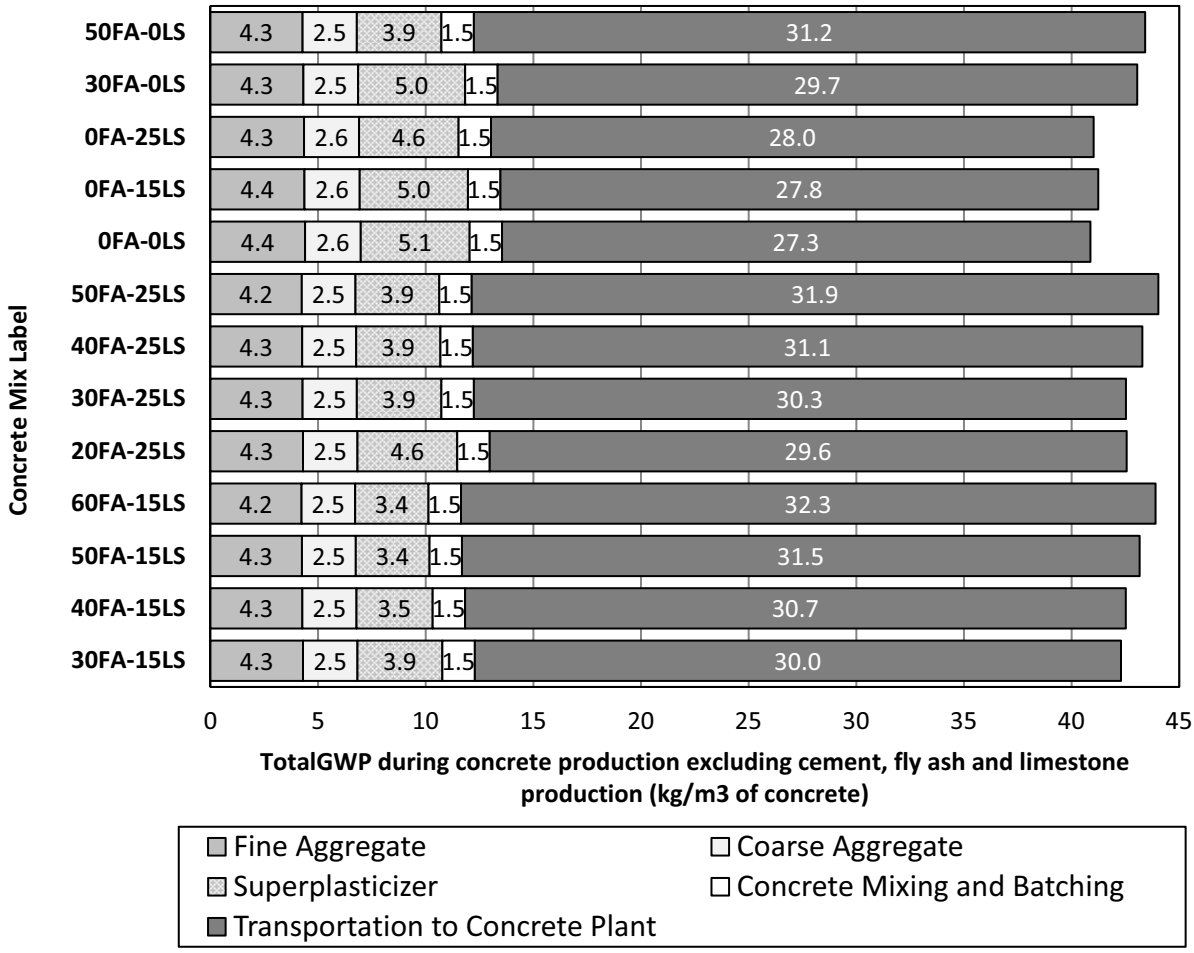

Figure 11. Total GWP associated with concrete production excluding cement, fly ash and limestone production (kg CO_2-eq / m^3 of concrete)

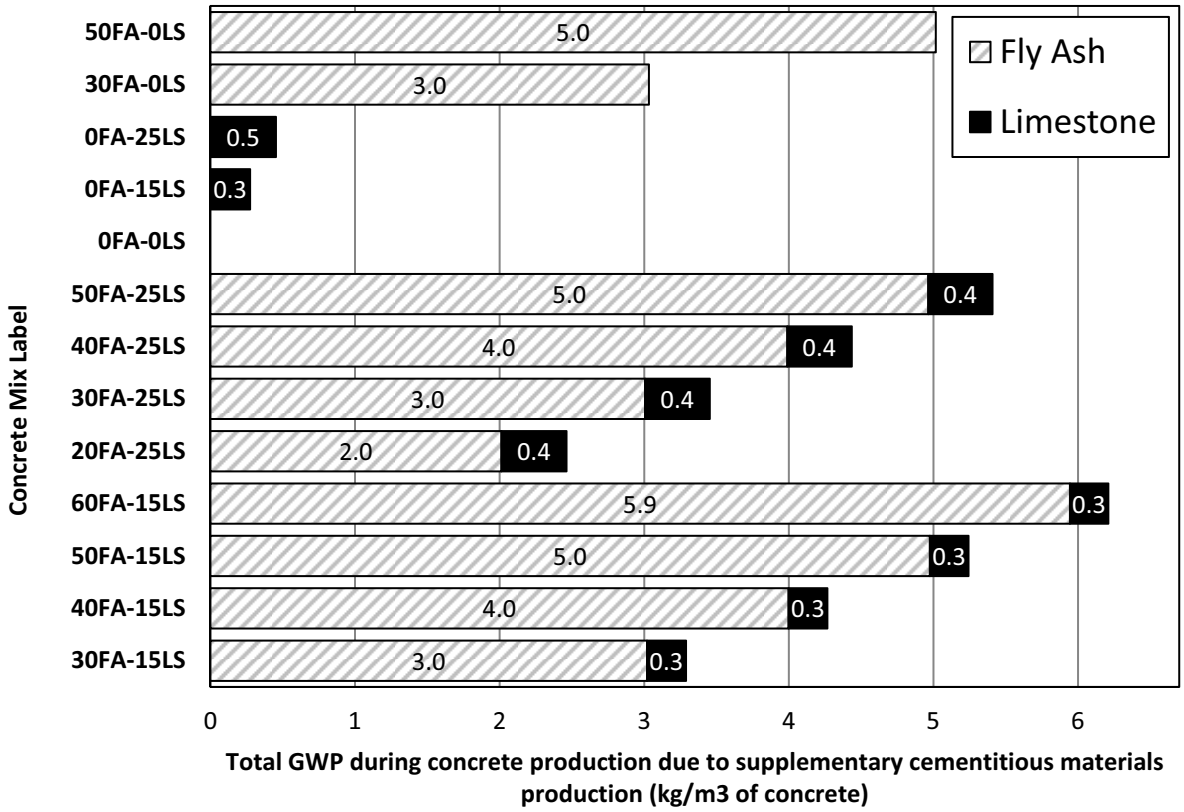

Figure 12. Total GWP associated with fly ash preparation and limestone production processes (kg CO_2-eq / m^3 of concrete)

Tables

Table 1. Particle size distribution of portland cement (C), limestone powder (L) and Class F fly ash (F).

	Mean (µm)	**Median (µm)**	**Mode (µm)**	**Standard Deviation (µm)**	**D10 (µm)**	**D50 (µm)**	**D90 (µm)**
C	**10.4**	**11.7**	**18.5**	**10.2**	**0.3**	**10.4**	**25.7**
F	**22.2**	**12.5**	**24.4**	**30.5**	**0.4**	**12.5**	**55.1**
L	**48.1**	**38.7**	**72.0**	**41.9**	**7.0**	**15.6**	**38.7**

Table 2. Chemical composition of powder materials (oxides, % by weight).

	C	F	L
SiO_2	20.44	62.0	0.70
Al_2O_3	3.97	18.90	0.50
Fe_2O_3	4.07	4.90	0.12
CaO	62.90	5.98	47.40
MgO	2.42	1.99	6.80
Na_2O	0.37	2.41	--
K_2O	0.43	1.14	--
P_2O_5	0.16	0.26	--
TiO_2	0.23	1.09	--
MnO	0.32	0.04	--
L.O.I.	4.69	1.30	44.48

Table 3. Concrete mix proportions

	(*w/cm* = 0.35)	Proportions (by weight)						kg/m^3 of concrete		
	C-F-L	C	F	L	Aggregates		SP (%)	CM	C	CR
					Fine	Coarse				
Control mixes	100-0-0	1.00	-	-	2.00	2.00	1.43	461	461	0
	85-0-15	0.85	-	0.15	2.00	2.00	1.43	458	389	69
	75-0-25	0.75	-	0.25	2.00	2.00	1.32	456	342	114
Binary HVFA blends	70-30-0	0.70	0.30	0.00	2.00	2.00	1.39	453	317	136
	50-50-0	0.50	0.50	0.00	2.00	2.00	1.14	449	224	225
Ternary HVFA-LS blends	55-30-15	0.55	0.30	0.15	2.00	2.00	1.14	451	248	203
	45-40-15	0.45	0.40	0.15	2.00	2.00	1.03	448	202	246
	35-50-15	0.35	0.50	0.15	2.00	2.00	1.00	446	156	290
	25-60-15	0.25	0.60	0.15	2.00	2.00	1.00	444	111	333
	55-20-25	0.55	0.2	0.25	2.00	2.00	1.34	451	248	203
	45-30-25	0.45	0.3	0.25	2.00	2.00	1.14	449	202	247
	35-40-25	0.35	0.4	0.25	2.00	2.00	1.14	447	156	291
	25-50-25	0.25	0.5	0.25	2.00	2.00	1.14	445	111	334

* Keys: *w/cm* = water/cementitious materials ratio; C = ordinary portland cement; F= Class F fly ash; L = limestone powder; SP = superplasticizer; CM = cementitious materials; CR = cement replacement.

Table 4. Assumptions for the concrete mix production LCA calculations*

User-Input Data:	**Assumption**	
Type of cement	Type I	
Type of SCMs	Fly ash, limestone	
Type of admixture	Superplasticizer	
Electricity grid mix for:	**Location**	
Cement supplier	California, US	
Fine aggregates supplier	California, US	
Coarse aggregates supplier	Canada, average	
Gypsum supplier	California, US	
Limestone supplier	California, US	
Fly ash supplier	Wyoming, US	
Transportation details for:	**Mode**	**Distance (km)**
Cement raw materials to cement plant	Truck_Class 8b (Model 2005)	1
Gypsum to cement plant	Truck_Class 8b (Model 2005)	200
Cement to concrete plant	Truck_Class 8b (Model 2005)	60
Fine aggregates to concrete plant	Truck_Class 8b (Model 2005)	50
Coarse aggregates to concrete plant	Water_Barge and Truck_Class 8b (Model 2005)	1,000 km by barge and 10 km by truck
Admixture to concrete plant	Truck_Class 8b (Model 2005)	1,000
Fly ash to concrete plant	Rail	1,000
Limestone to concrete plant	Truck_Class 8b (Model 2005)	130
Technology options for:	**Type of technology selected**	**Distance (m)**
Cement raw materials prehomogenization	Dry, raw storing, preblending	
Cement raw materials grinding	Dry, raw grinding, ball mill	
Cement raw meal blending/homogenization	Dry, raw meal blending, storage	
Clinker pyroprocessing	Preheater/Precalciner kiln with US average kiln fuel mix [75]	
Clinker cooling	Reciprocating grate cooler (modern)	
Cement finish milling/grinding/blending	Roller press	
Cement PM control technology	ESP	
Conveying within the cement plant	Screw pump	20 m between process stations
Concrete batching plant loading/mixing	Mixer loading (central mix)	
Concrete batching plant PM control	Fabric filter	

* For further details see GreenConcrete LCA tool (Website: http://greenconcrete.berkeley.edu/).

Table 5. Electricity grid mix percentage by source of energy adapted from EIA [65, 66] for United States and from CEA [67] for Canada

User-Input Data	California (%)	Wyoming (%)	Canada (%)
Coal	1	91	19
Natural gas	55	1	6
Fuel oil	0.1	0.1	3
Petroleum coke	1		
Nuclear	16		13
Hydropower	14	2	58
Biomass	3		
Geothermal	6		
Solar	0.3		1
Wind	3	5	

* Percentages may not add up to 100% because rounding of the numbers during calculations.

Table 6. Setting time of the mixes

	C-F-L	w/cm for normal consistency	Setting time, minutes	
			Initial	Final
Control mixes	100-0-0	0.25	136	185
	85-0-15	0.25	134	185
	75-0-25	0.25	128	185
Binary HVFA blends	70-30-0	0.23	189	260
	50-50-0	0.22	353	420
Ternary HVFA-LS blends	55-30-15	0.24	267	315
	45-40-15	0.22	282	345
	35-50-15	0.22	340	360
	25-60-15	0.21	278	390
	55-20-25	0.24	214	270
	45-30-25	0.23	245	300
	35-40-25	0.22	285	345
	25-50-25	0.22	359	405

Table 7. Slump flow diameter and T_{50}.

C-F-L	d_s (mm)	T_{50} (sec.)	SP (%)
100-0-0	584	4.5	1.43
85-0-15	622	4.4	1.43
75-0-25	559	4.6	1.32
70-30-0	610	4.5	1.43
50-50-0	660	3.8	1.14
55-30-15	622	3.6	1.14
45-40-15	572	3.2	1.03
35-50-15	635	2.6	1.00
25-60-15	667	2.8	1.00
55-20-25	635	4.0	1.34
45-30-25	622	3.8	1.14
35-40-25	653	3.0	1.14
25-50-25	692	3.5	1.14

Table 8. Specifications and recommended values for SCC [52]

Workability characteristic	**Test Methods**	**Recommended Values**
Deformability and flow rate (filling ability, unrestricted flow)	Slump flow	Hwang et al .620 mm to 720 mm EFNARC: 650 mm to 800 mm JSCE: 600 mm to 700 mm PCI: ≥ 660 mm Swedish Concrete Association: 650 mm to 750 mm
	T_{50}	EFNARC: 2-5 seconds PCI: 3-5 seconds Swedish Concrete Association: 3-7 seconds

Table 9. Average compressive strength (MPa).

C-F-L	Compressive Strength (MPa)			
	7 days	**28 days**	**91 days**	**365 days**
100-0-0	43.9	53.9	66.3	77.1
85-0-15	28.0	43.2	49.7	53.0
75-0-25	22.2	33.6	38.7	42.2
70-30-0	35.6	51.0	64.6	71.8
50-50-0	27.9	41.6	54.8	64.8
55-30-15	21.5	37.5	47.3	56.8
45-40-15	17.1	33.9	46.2	56.5
35-50-15	12.9	26.0	39.3	49.0
25-60-15	10.3	20.6	29.4	39.5
55-20-25	19.6	36.3	42.9	54.2
45-30-25	14.9	31.5	43.3	55.3
35-40-25	12.4	28.9	41.8	50.4
25-50-25	10.1	20.6	32.8	38.0

Table 10. Resistance against chloride penetration based on non-steady state migration testing [54]

Chloride Diffusion D ($\times 10^{-12}$ m^2/s)	**Concrete Resistance**
> 15	Low
10 – 15	Moderate
5 – 10	High
2.5 – 5	Very high
< 2.5	Extremely high

Table 11 Material GWP, and criteria air pollutants

C-F-L	CO_2-eq (kg /m^3)	CO (kg /m^3)	NO_X (kg /m^3)	PMtotal (kg /m^3)	SO_2 (kg /m^3)
100-0-0	5.69E+02	1.35E-01	2.99E+00	3.64E-01	1.35E+00
85-0-15	4.87E+02	1.26E-01	2.61E+00	3.09E-01	1.15E+00
75-0-25	4.34E+02	1.20E-01	2.36E+00	2.73E-01	1.03E+00
70-30-0	4.12E+02	1.49E-01	2.27E+00	2.62E-01	9.74E-01
50-50-0	3.11E+02	1.57E-01	1.82E+00	1.97E-01	7.31E-01
55-30-15	3.33E+02	1.39E-01	1.91E+00	2.09E-01	7.84E-01
45-40-15	2.82E+02	1.43E-01	1.68E+00	1.77E-01	6.63E-01
35-50-15	2.32E+02	1.47E-01	1.45E+00	1.44E-01	5.44E-01
25-60-15	1.83E+02	1.52E-01	1.23E+00	1.12E-01	4.27E-01
55-20-25	3.32E+02	1.29E-01	1.90E+00	2.07E-01	7.83E-01
45-30-25	2.81E+02	1.33E-01	1.67E+00	1.74E-01	6.61E-01
35-40-25	2.31E+02	1.38E-01	1.44E+00	1.42E-01	5.42E-01
25-50-25	1.82E+02	1.43E-01	1.22E+00	1.10E-01	4.26E-01

References

[1] USGS, Cement - Mineral Commodity Summaries, in: Cement Statistics and Information - Annual Publications, U.S. Department of the Interior, U.S. Geological Survey, 2011.
[2] P.K. Mehta, P.J.M. Monteiro, Concrete: Microstructure, Properties, and Materials, 4th Edition ed., McGraw-Hill, USA, 2014.
[3] WBCSD-CSI, Cement Industry Energy and CO_2 Performance "Getting the Numbers Right", in, Washington DC, 2009.
[4] M.L. Marceau, M.A. Nisbet, M.G. VanGeem, Life Cycle Inventory of Portland Cement Manufacture, in, Portland Cement Association [PCA], Skokie, IL, 2006.
[5] D. Bonen, S.P. Shah, Fresh and hardened properties of self-consolidating concrete, Progress in Structural Engineering and Materials, 7 (2005) 14-26.
[6] C.D. Tomkins, Redefining What's Possible for Clean Energy by 2020, in, Gigaton Throwdown, San Francisco, 2009.
[7] P.K. Mehta, Global Concerete Industry Sustainability: Tools for Moving Forward to Cut Carbon Emissions, Concrete International, (2009) 45-48.
[8] V.M. Malhotra, High-Performance High-Volume Fly Ash Concrete, Concrete International, 24 (2002) 30-34.
[9] P.K. Mehta, D. Manmohan, Sustainable High-Performance Concrete Structures, Concrete International, 28 (2006) 37-42.
[10] P.K. Mehta, Sustainable Cements and Concrete for the Climate Change Era – A Review, in: P.C. Zachar, T R Naik, E Ganjian (Ed.) Second International Conference on Sustainable Construction Materials and Technologies, Coventry University and The University of Wisconsin Milwaukee Centre for By-products Utilization,, Italy, 2010.
[11] D.P. Bentz, E.F. Irassar, B.E. Bucher, J. Weiss, Limestone Fillers Conserve Cement Part 1: An analysis based on Powers' model, Concr Int, (2009).
[12] D.P. Bentz, E.F. Irassar, B.E. Bucher, W.J. Weiss, Limestone Fillers Conserve Cement Part 2: Durability issues and the effects of limestone fineness on mixtures, Concr Int, December (2009) 35-39.
[13] T. Matschei, B. Lothenbach, F.P. Glasser, The role of calcium carbonate in cement hydration, Cem Concr Res, 37 (2007) 551-558.
[14] A.-M. Poppe, G. De Schutter, Cement hydration in the presence of high filler contents, Cem Concr Res, 35 (2005) 2290-2299.
[15] A. Ipavec, R. Gabrovšek, T. Vuk, V. Kaučič, J. Maček, A. Meden, Carboaluminate Phases Formation During the Hydration of Calcite-Containing Portland Cement, Journal of the American Ceramic Society, 94 (2011) 1238-1242.
[16] B. Lothenbach, G. Le Saout, E. Gallucci, K. Scrivener, Influence of Limestone on the Hydration of Portland Cements, Cem Concr Res, 38 (2008) 848-860.

[17] V. Bonavetti, H. Donza, V. Rahhal, E. Irassar, Influence of initial curing on the properties of concrete containing limestone blended cement, Cement and Concrete Research, 30 (2000) 703-708.
[18] M. Ouchi, S. Nakamura, T. Osterson, S. Hallberg, M. Lwin, Applications of Self-Compacting Concrete in Japan, Europe and the United States, in: International Symposium on High Performance Concrete, Orlando, FL, 2003, pp. 20.
[19] A.W. Saak, H.M. Jennings, S.P. Shah, New Methodology For Designing Self-Compacting Concrete, ACI Materials Journal, 98 (2001) 429-439.
[20] A.W.J. Saak, H.M.; Shah,S.P., A, A generalized approach for the determination of yield stress by slump and slump flow, Cement and Concrete Research, 34 (2004) 363-371.
[21] G. Le Saoût, V. Kocaba, K. Scrivener, Application of the Rietveld method to the analysis of anhydrous cement, Cement and Concrete Research, 41 (2011) 133-148.
[22] C.W. Hargis, J. Moon, B. Lothenbach, F. Winnefeld, H.-R. Wenk, P.J.M. Monteiro, Calcium Sulfoaluminate Sodalite (Ca4Al6O12SO4) Crystal Structure Evaluation and Bulk Modulus Determination, Journal of the American Ceramic Society, (2013) n/a-n/a.
[23] A.P. Gursel, A. Horvath, GreenConcrete LCA Tool, in, University of California, Berkeley, Berkeley, CA, 2012.
[24] G. Rebitzer, T. Ekvall, R. Frischknecht, D. Hunkeler, G. Norris, T. Rydberg, W.P. Schmidt, S. Suh, B.P. Weidema, D.W. Pennington, Life cycle assessment: Part 1: Framework, goal and scope definition, inventory analysis, and applications, Environment International, 30 (2004) 701-720.
[25] C. Meral, C.J. Benmore, P.J.M. Monteiro, The study of disorder and nanocrystallinity in C–S–H, supplementary cementitious materials and geopolymers using pair distribution function analysis, Cement and Concrete Research, 41 (2011) 696-710.
[26] S.A. Bilgrami, Serpentinite-limestone contact at Taleri Mohammad Jan, Zhob Valley, , West Pakistan, The American Mineralogist, 45 (1960) 1008-1019.
[27] D.N. Lumsden, Discrepancy between thin-section and X-ray estimates of dolomite in limestone, Journal of Sedimentary Research, 49 (1979) 429-435.
[28] G. Durn, F. Ottner, D. Slovenec, Mineralogical and geochemical indicators of the polygenetic nature of terra rossa in Istria, Croatia, Geoderma, 91 (1999) 125-150.
[29] ASTM, C192/C192M – 07 Standard Practice for Making and Curing Concrete Test Specimens in the Laboratory1, in: Safety Precautions, Manual of Aggregate and Concrete Testing, Annual Book of ASTM Standards, ASTM, 2007, pp. 1-8.
[30] B. Pekmezci, Optimum usage of a natural pozzolan for the maximum compressive strength of concrete, Cement and Concrete Research, 34 (2004) 2175-2179.
[31] P.K. Mehta, Reducing the Environmental Impact of Concrete, Concrete International, 23 (2001) 61-66.
[32] ASTM, C1611/C1611M – 09b Standard Test Method for Slump Flow of Self-Consolidating Concrete, in, ASTM, 2009, pp. 1-6.

[33] S.E.P. Group, The European Guidelines for Self Compacting Concrete, in, 2005.
[34] E.P. Koehler, D.W. Fowler, Inspection manual for self-consolidating concrete in precast members, in, Center for Transportation Research The University of Texas at Austin, 2007.
[35] K. Celik, M.D. Jackson, M. Mancio, C. Meral, A.H. Emwas, P.K. Mehta, P.J.M. Monteiro, High-volume natural volcanic pozzolan and limestone powder as partial replacements for portland cement in self-compacting and sustainable concrete, Cement and Concrete Composites, 45 (2014) 136-147.
[36] ASTM, C39/C39M – 10 Standard Test Method for Compressive Strength of Cylindrical Concrete Specimens, in, ASTM, 2010, pp. 1-7.
[37] ASTM, C1231/C1231M-12 Standard Practice for Use of Unbonded Caps in Determination of Compressive Strength of Hardened Concrete Cylinders, in, ASTM, 2012, pp. 1-5.
[38] ASTM, C617/C617M-12 Standard Practice for Capping Cylindrical Concrete Specimens, in, 2012, pp. 1-6.
[39] S.A. Issa, M.S. Islam, M.A. Issa, A.A. Yousif, M.A. Issa, Specimen and Aggregate Size Effect on Concrete Compressive Strength, Cem Concr Aggr, 22 (2000) 103-115.
[40] M. Tokyay, Ozdemir, M., Specimen shape and size effect on the compressive strength of higher strength concrete, Cem Concr Res, 27 (1997) 1281-1289.
[41] NORDTEST, NT BUILD 492: Concrete, mortar and cement-based repair materials: chloride migration coefficient from non-steady-state migration experiments, in, Nordtest, Finland, 1999, pp. 1-8.
[42] RILEM, RILEM TC 116-PCD: Permeability of concrete as a criterion of its durability Materials and Structures, 32 (1999) 174-179.
[43] J.J. Kollek, The determination of the permeability of concrete to oxygen by the Cembureau method- a recommendation, Materials and Structures, 22 (1989) 225-230.
[44] A. Petek Gursel, E. Masanet, A. Horvath, A. Stadel, Life-cycle inventory analysis of concrete production: A critical review, Cement and Concrete Composites, 51 (2014) 38-48.
[45] ISO, Environmental management - Life Cycle Assessment: Principles and Framework. ISO 14040:2006, in, International Organization for Standardization, Geneva, Switzerland, 2006a.
[46] ISO, Environmental management - Life Cycle Assessment: Requirements and Guidelines. ISO 14044:2006, in, International Organization for Standardization, Geneva, Switzerland, 2006b.
[47] EPA, Life Cycle Assessment: Principles and Practice, in, U.S. Environmental Protection Agency - National Risk Management Research Laboratory, Office of Research and Development, Cincinnati, Ohio, 2006.
[48] IPCC, IPCC Guidelines for National Greenhouse Gas Inventories, in, Intergovernmental Panel on Climate Change - National Greenhouse Gas Inventories Programme Technical Support Unit Geneva, Switzerland, 2006.

[49] IPCC, Climate Change 2007: The Physical Science Basis, in: C.U. Press (Ed.) Contribution of Working Group I to the Fourth Assessment Report of the Intergovernmental Panel on Climate Change, World Meteorological Organization (WMO) and the United Nations Environment Programme (UNEP), Cambridge, United Kingdom, 2007, pp. 996.
[50] S. Hans-Henning, Fundamentals of Corrosion, in: Corrosion Mechanisms in Theory and Practice, Third Edition, CRC Press, 2011, pp. 1-104.
[51] C. Hendrickson, L. Lave, S. Matthews, Environmental Life Cycle Assessment of Goods and Services-An Input-Output Approach, Resources for the Future, Washington, D.C., 2006.
[52] A. Abbas, M. Carcasses, J.P. Ollivier, The importance of gas permeability in addition to the compressive strength of concrete, Mag Concrete Res, 52 (2000) 1-6.
[53] N. Diamantonis, I. Marinos, M.S. Katsiotis, A. Sakellariou, A. Papathanasiou, V. Kaloidas, M. Katsioti, Investigations about the influence of fine additives on the viscosity of cement paste for self-compacting concrete, Construction and Building Materials, 24 (2010) 1518-1522.
[54] O.E. Gjørv, Durability design of concrete structures in severe environments, in, Taylor & Francis, New York, 2009.
[55] K.E. Hassan, J.G. Cabrera, R.S. Maliehe, The effect of mineral admixtures on the properties of high-performance concrete, Cem Concr Compos, 22 (2000) 267-271.
[56] A. Abbas, M. Carcasses, P.P. Ollivier, Gas permeability of concrete in relation to its degree of saturation, Materials and Structures, 32 (1999) 3-8.
[57] T. Sugiyama, T.W. Bremner, T.A. Holm, Effect of Stress on Gas Permeability in Concrete, ACI Mater J, 93 (1996) 443-450.
[58] T. Sugiyama, T.W. Bremner, Y. Tsuji, Determination of chloride diffusion coefficient and gas permeability of concrete and their relationship, Cem Concr Res, 26 (1996) 781-790.
[59] H. Okamura, M. Ouchi, Self-compacting concrete, J Adv Concr Technol 1(2003) 5-15.
[60] M. Şahmaran, İ.Ö. Yaman, M. Tokyay, Transport and mechanical properties of self consolidating concrete with high volume fly ash, Cement and Concrete Composites, 31 (2009) 99-106.
[61] B.L. Damineli, F.M. Kemeid, P.S. Aguiar, V.M. John, Measuring the eco-efficiency of cement use, Cement and Concrete Composites, 32 (2010) 555-562.
[62] B. Lothenbach, K. Scrivener, R.D. Hooton, Supplementary cementitious materials, Cement and Concrete Research, 41 (2011) 1244-1256.
[63] C. Chen, G. Habert, Y. Bouzidi, A. Jullien, A. Ventura, LCA allocation procedure used as an incitative method for waste recycling: An application to mineral additions in concrete, Resources, Conservation and Recycling, 54 (2010) 1231-1240.

[64] A. Barker, H. Cory, The early hydration of limestone-filled cements., in: R.N. Swamy (Ed.) Blended Cements in Construction, Elsevier Science, London, 1991, pp. 107-124.
[65] EIA, Electricity Net Generation by State by Type of Producer by Energy Source, Annual Back to 1990 (EIA-906, EIA-920, and EIA-923), in, U.S. Energy Information Administration Washington, DC, 2011g.
[66] H.-s. Shi, B.-w. Xu, X.-c. Zhou, Influence of mineral admixtures on compressive strength, gas permeability and carbonation of high performance concrete, Construction and Building Materials, 23 (2009) 1980-1985.
[67] CEA, Canadian Electricity Association - Industry Data, in, 2012.